

Fast Bayesian approach for modal identification using free vibration data, Part II – Posterior uncertainty and application

Yan-Chun Ni^{1*}, Feng-Liang Zhang¹, Heung-Fai Lam² and Siu-Kui Au³

¹Research Institute of Structural Engineering and Disaster Reduction, College of Civil Engineering, Tongji University

²Department of Civil and Architectural Engineering, City University of Hong Kong

³Centre for Engineering Dynamics and Institute for Risk and Uncertainty, University of Liverpool

Abstract: A Bayesian statistical framework has been developed for modal identification using free vibration data in the companion paper [1]. Efficient strategies have been developed for evaluating the most probable value (MPV) of the modal parameters in both well-separated mode and general multiple mode cases. This paper investigates the posterior uncertainty of the modal parameters in terms of their posterior covariance matrix, which is mathematically equal to the inverse of the Hessian of the negative log-likelihood function (NLLF) evaluated at the MPVs. Computational issues associated with the determination of the posterior covariance matrix are discussed. Analytical expressions are derived for the Hessian so that it can be evaluated accurately and efficiently without resorting to finite difference method. The proposed methods are verified with synthetic data and then applied to field vibration test data.

Keywords: Free vibration, modal identification, posterior uncertainty, field test, application

* Corresponding author. Tel.: +86 021 65987352; E-mail address: yanchunni@gmail.com

1. Introduction

In addition to the most probable value (MPV) of the modal parameters, a Bayesian identification approach also yields their posterior uncertainties, which is a fundamental quantification of their remaining uncertainties in the presence of the data and consistent with modeling assumptions [2]-[6]. Quantifying the uncertainties is especially relevant in the field testing setting because the identification results are subjected to a variety of uncertainties, e.g., channel noise, unknown environmental disturbances, unknown environmental changes, modeling error associated with the identification model [7]-[10].

Fast Bayesian methods for calculating the posterior uncertainties of identified modal parameters based on ambient and forced data have been developed and applied in practice recently [5][11][12][13]. In Part I of this work [1], efficient methods have been developed for evaluating the MPV of modal parameters using free vibration data in both well-separated mode and general multiple mode cases. In this paper the posterior covariance matrix of the modal parameters is investigated and it can be calculated as the inverse of the Hessian of the negative log-likelihood function (NLLF) evaluated at the MPV of modal parameters. Computational issues exist in the evaluation of the inverse and they will be discussed first. Analytical expressions for the Hessian will be derived so that it can be evaluated accurately and efficiently without resorting to finite difference method. The proposed methods will be verified using synthetic data. Parametric studies will be performed with respect to effects of channel noise and ambient vibration levels. Application to field data will also be presented to illustrate the applicability of the proposed methods.

This paper is organized as follows. In Section 2, the computational issues associated with evaluating the posterior covariance matrix for modal parameters are addressed. Section 3 presents the analytical expressions for the Hessian of the NLLF in well-separated mode case. In Section 4, the analytical expressions for the Hessian of the NLLF in general multiple modes case are investigated. The verification using synthetic data are presented in Section 5. In Section 6, the proposed methods are applied in the field data, including two footbridges situated in Singapore and Hong Kong respectively. The paper is concluded in Section 7. Section 8 shows some derivation used in the analytical expressions of Section 3.

2. Computational issues

The basic computational issues associated with evaluating the posterior covariance matrix for modal parameters arise from the norm constraint of the mode shapes. The issues have been investigated in [5] and they are briefly outlined here.

Recall that the mode shapes $\{\Phi(i) \in R^n : i = 1, \dots, m\}$ are subjected to unit norm constraint, i.e.,

$$\|\Phi(i)\|^2 = \Phi(i)^T \Phi(i) = 1 \quad (1)$$

These constraints have been taken into account in the determination of MPV. One strategy to correctly reflect the constraint in the determination of the Hessian of the NLLF is to write the mode shape explicitly in normalized form. That is, let

$$\bar{\Phi}(i) = \|\Phi(i)\|^{-1} \Phi(i) \quad (2)$$

and then it is clear that $\|\bar{\Phi}(i)\| = 1$ regardless of $\Phi(i)$. For the determination of Hessian, the mode shape $\Phi(i)$ contained in the expression of the NLLF in (14) of the companion paper [1] should be replaced by $\bar{\Phi}(i)$ so that the NLLF can be differentiated with respect to the free parameters in $\Phi(i)$ without any constraint. By this construction, the resulting NLLF will be invariant to the scaling of $\Phi(i)$. Correspondingly the Hessian of the NLLF will be singular along the directions $\{\Phi(i) : i = 1, \dots, m\}$. It will thus have m zero eigenvalues along the eigen-directions $\{\Phi(i) : i = 1, \dots, m\}$ and is therefore not invertible. However, it can be reasoned that this singularity is immaterial to the evaluation of the posterior covariance matrix, because the mode shape uncertainties are orthogonal to such directions by definition. Let $\{\lambda_i : i = 1, \dots, n_p\}$ and $\{\mathbf{w}_i \in R^{n_p} : i = 1, \dots, n_p\}$ be respectively the eigenvalues (in ascending order) and eigenvectors of the Hessian matrix of the NLLF at the MPV. Then the Hessian has the eigenvector representation

$$\mathbf{H}_L = \sum_{i=m+1}^{n_p} \lambda_i \mathbf{w}_i \mathbf{w}_i^T \quad (3)$$

since $\lambda_1 = \dots = \lambda_m = 0$. Ignoring the singular directions, the posterior covariance matrix as the inverse of \mathbf{H}_L is evaluated as

$$\mathbf{C} = \sum_{i=m+1}^{n_p} \lambda_i^{-1} \mathbf{w}_i \mathbf{w}_i^T \quad (4)$$

Next, we shall present the terms in the Hessian matrix of the NLLF. The discussion is separated into two sections as the NLLF for well-separated modes and general multiple modes (ignoring ambient vibration) is somewhat different and involves a different set of modal parameters. In order to have a better understanding, the derivatives of the following formulations are consistent with the ones in other papers about Bayesian methods developed by the same group.

3. Hessian for well-separated modes

For well-separated modes, i.e., a single mode in the selected frequency band, the NLLF is given by (21) of the companion paper [1] (in terms of normalized mode shape).

$$\begin{aligned} L(\boldsymbol{\theta}) = & nN_f \ln \pi + (n-1)N_f \ln S_e + \sum_k \ln(SD_k + S_e) \\ & + S_e^{-1} \left[d - \frac{\boldsymbol{\phi}^T \mathbf{A} \boldsymbol{\phi}}{\|\boldsymbol{\phi}\|^2} + \sum_k (1-a_k)(b_{Rk}^2 + b_{Ik}^2) - 2 \frac{\boldsymbol{\phi}^T}{\|\boldsymbol{\phi}\|} \sum_k (1-a_k)(b_{Rk} \operatorname{Re} \mathcal{F}_k + b_{Ik} \operatorname{Im} \mathcal{F}_k) \right] \end{aligned} \quad (5)$$

where $\boldsymbol{\phi} \in R^n$ denotes the mode shape vector.

The Hessian matrix can be determined by the second derivatives of the NLLF with respect to parameter set $\{f, \zeta, S, S_e, u, v, \boldsymbol{\phi}\}$, whose dimension is $(n+6) \times (n+6)$. The details for calculating the Hessian matrix are presented as follows. For simplicity we denote the variable under differentiation by a superscript in parenthesis. Only the derivatives of the NLLF L are presented here. The derivatives of other parameters, e.g., $a_k^{(ff)}$, are given in the Appendix.

The second derivative of L with respect to f is given by

$$\begin{aligned}
L^{(ff)} = & \sum_k [a_k D_k^{-1} D_k^{(ff)} - a_k^2 (D_k^{-1} D_k^{(f)})^2] + S_e^{-1} \left\{ -\sum_k a_k^{(ff)} \frac{\boldsymbol{\Phi}^T \mathbf{D}_k \boldsymbol{\Phi}}{\|\boldsymbol{\Phi}\|^2} \right. \\
& + \sum_k 2(1-a_k) [b_{Rk}^{(ff)} b_{Rk} + b_{Ik}^{(ff)} b_{Ik} + (b_{Rk}^{(f)})^2 + (b_{Ik}^{(f)})^2] - \sum_k 4a_k^{(f)} [b_{Rk}^{(f)} b_{Rk} + b_{Ik}^{(f)} b_{Ik}] \\
& - \sum_k a_k^{(ff)} (b_{Rk}^2 + b_{Ik}^2) + 2 \frac{\boldsymbol{\Phi}^T}{\|\boldsymbol{\Phi}\|} \sum_k a_k^{(ff)} (b_{Rk} \operatorname{Re} \mathcal{F}_k + b_{Ik} \operatorname{Im} \mathcal{F}_k) \\
& \left. + 4 \frac{\boldsymbol{\Phi}^T}{\|\boldsymbol{\Phi}\|} \sum_k a_k^{(f)} (b_{Rk}^{(f)} \operatorname{Re} \mathcal{F}_k + b_{Ik}^{(f)} \operatorname{Im} \mathcal{F}_k) - 2 \frac{\boldsymbol{\Phi}^T}{\|\boldsymbol{\Phi}\|} \sum_k (1-a_k) (b_{Rk}^{(ff)} \operatorname{Re} \mathcal{F}_k + b_{Ik}^{(ff)} \operatorname{Im} \mathcal{F}_k) \right\}
\end{aligned} \tag{6}$$

The expression of $L^{(\zeta\zeta)}$ is similar to $L^{(ff)}$.

The second derivative of L with respect to S is given by

$$\begin{aligned}
L^{(SS)} = & -S^{-2} \sum_k a_k^2 + S_e^{-1} \left[-\sum_k a_k^{(SS)} \frac{\boldsymbol{\Phi}^T \mathbf{D}_k \boldsymbol{\Phi}}{\|\boldsymbol{\Phi}\|^2} - \sum_k a_k^{(SS)} (b_{Rk}^2 + b_{Ik}^2) \right. \\
& \left. + 2 \frac{\boldsymbol{\Phi}^T}{\|\boldsymbol{\Phi}\|} \sum_k a_k^{(SS)} (b_{Rk} \operatorname{Re} \mathcal{F}_k + b_{Ik} \operatorname{Im} \mathcal{F}_k) \right]
\end{aligned} \tag{7}$$

The second derivative of L with respect to S_e is given by

$$\begin{aligned}
L^{(S_e S_e)} = & -S_e^{-2} [(n-1)N_f + \sum_k \left(\frac{S_e}{SD_k}\right)^2 a_k^2] + 2S_e^{-3} \left[d - \frac{\boldsymbol{\Phi}^T \mathbf{A} \boldsymbol{\Phi}}{\|\boldsymbol{\Phi}\|^2} + \sum_k (1-a_k) (b_{Rk}^2 + b_{Ik}^2) \right. \\
& - 2 \frac{\boldsymbol{\Phi}^T}{\|\boldsymbol{\Phi}\|} \sum_k (1-a_k) (b_{Rk} \operatorname{Re} \mathcal{F}_k + b_{Ik} \operatorname{Im} \mathcal{F}_k) \\
& - 2S_e^{-2} \left[-\sum_k a_k^{(S_e)} \frac{\boldsymbol{\Phi}^T \mathbf{D}_k \boldsymbol{\Phi}}{\|\boldsymbol{\Phi}\|^2} - \sum_k a_k^{(S_e)} (b_{Rk}^2 + b_{Ik}^2) + 2 \frac{\boldsymbol{\Phi}^T}{\|\boldsymbol{\Phi}\|} \sum_k a_k^{(S_e)} (b_{Rk} \operatorname{Re} \mathcal{F}_k + b_{Ik} \operatorname{Im} \mathcal{F}_k) \right] \\
& \left. + S_e^{-1} \left[-\sum_k a_k^{(S_e S_e)} \frac{\boldsymbol{\Phi}^T \mathbf{D}_k \boldsymbol{\Phi}}{\|\boldsymbol{\Phi}\|^2} - \sum_k a_k^{(S_e S_e)} (b_{Rk}^2 + b_{Ik}^2) + 2 \frac{\boldsymbol{\Phi}^T}{\|\boldsymbol{\Phi}\|} \sum_k a_k^{(S_e S_e)} (b_{Rk} \operatorname{Re} \mathcal{F}_k + b_{Ik} \operatorname{Im} \mathcal{F}_k) \right] \right]
\end{aligned} \tag{8}$$

The second derivative of L with respect to u is given by

$$L^{(uu)} = S_e^{-1} \sum_k 2(1-a_k) [(b_{Rk}^{(u)})^2 + (b_{Ik}^{(u)})^2] \tag{9}$$

The expression of $L^{(vv)}$ is similar to $L^{(uu)}$.

The second derivative of L with respect to $\boldsymbol{\Phi}$ is given by

$$L^{(\Phi\Phi)} = S_e^{-1} \left(-\frac{2\mathbf{A}}{\|\Phi\|^2} + \frac{4\Phi\Phi^T\mathbf{A}}{\|\Phi\|^4} - \frac{8\Phi^T\mathbf{A}\Phi\Phi\Phi^T}{\|\Phi\|^6} + \frac{4\mathbf{A}\Phi\Phi^T}{\|\Phi\|^4} + \frac{2\Phi^T\mathbf{A}\Phi}{\|\Phi\|^4} \mathbf{I}_n + \mathbf{P} \right) \quad (10)$$

where the (r_1, r_2) ($r_1, r_2 = 1, \dots, n$) entry of \mathbf{P} is given by

$$\mathbf{P}(r_1, r_2) = -2(\bar{\Phi}^{(\phi_{r_1}\phi_{r_2})})^T \sum_k (1-a_k)(b_{Rk} \operatorname{Re} \mathcal{F}_k + b_{Ik} \operatorname{Im} \mathcal{F}_k) \quad (11)$$

where $\phi_{r_1} \in R$ denotes the r_1 -entry of mode shape vector Φ ; the second derivative $\bar{\Phi}^{(\phi_{r_1}\phi_{r_2})}$ can be calculated according to (52).

The cross derivative of L with respect to f and ζ is given by

$$\begin{aligned} L^{(f\zeta)} = & \sum_k [a_k D_k^{-1} D_k^{(f\zeta)} - a_k^2 D_k^{-2} D_k^{(f)} D_k^{(\zeta)}] + S_e^{-1} \left\{ -\sum_k a_k^{(f\zeta)} \frac{\Phi^T \mathbf{D}_k \Phi}{\|\Phi\|^2} \right. \\ & + \sum_k 2(1-a_k) [b_{Rk}^{(f\zeta)} b_{Rk} + b_{Ik}^{(f\zeta)} b_{Ik} + b_{Rk}^{(f)} b_{Rk}^{(\zeta)} + b_{Ik}^{(f)} b_{Ik}^{(\zeta)}] - \sum_k 2a_k^{(\zeta)} [b_{Rk}^{(f)} b_{Rk} + b_{Ik}^{(f)} b_{Ik}] \\ & - \sum_k 2a_k^{(f)} [b_{Rk}^{(\zeta)} b_{Rk} + b_{Ik}^{(\zeta)} b_{Ik}] - \sum_k a_k^{(f\zeta)} (b_{Rk}^2 + b_{Ik}^2) + 2 \frac{\Phi^T}{\|\Phi\|} \sum_k a_k^{(f\zeta)} (b_{Rk} \operatorname{Re} \mathcal{F}_k + b_{Ik} \operatorname{Im} \mathcal{F}_k) \\ & + 2 \frac{\Phi^T}{\|\Phi\|} \sum_k a_k^{(f)} (b_{Rk}^{(\zeta)} \operatorname{Re} \mathcal{F}_k + b_{Ik}^{(\zeta)} \operatorname{Im} \mathcal{F}_k) + 2 \frac{\Phi^T}{\|\Phi\|} \sum_k a_k^{(\zeta)} (b_{Rk}^{(f)} \operatorname{Re} \mathcal{F}_k + b_{Ik}^{(f)} \operatorname{Im} \mathcal{F}_k) \\ & \left. - 2 \frac{\Phi^T}{\|\Phi\|} \sum_k (1-a_k) (b_{Rk}^{(f\zeta)} \operatorname{Re} \mathcal{F}_k + b_{Ik}^{(f\zeta)} \operatorname{Im} \mathcal{F}_k) \right\} \quad (12) \end{aligned}$$

The cross derivative of L with respect to f and S is given by

$$\begin{aligned} L^{(fS)} = & \sum_k \left[\frac{S_e}{(SD_k + S_e)^2} D_k^{(f)} \right] + S_e^{-1} \left[-\sum_k a_k^{(fS)} \frac{\Phi^T \mathbf{D}_k \Phi}{\|\Phi\|^2} - \sum_k 2a_k^{(S)} (b_{Rk}^{(f)} b_{Rk} + b_{Ik}^{(f)} b_{Ik}) \right. \\ & - \sum_k a_k^{(fS)} (b_{Rk}^2 + b_{Ik}^2) + 2 \frac{\Phi^T}{\|\Phi\|} \sum_k a_k^{(fS)} (b_{Rk} \operatorname{Re} \mathcal{F}_k + b_{Ik} \operatorname{Im} \mathcal{F}_k) \\ & \left. + 2 \frac{\Phi^T}{\|\Phi\|} \sum_k a_k^{(S)} (b_{Rk}^{(f)} \operatorname{Re} \mathcal{F}_k + b_{Ik}^{(f)} \operatorname{Im} \mathcal{F}_k) \right] \quad (13) \end{aligned}$$

The expression of $L^{(\zeta S)}$ is similar to $L^{(fS)}$.

The cross derivative of L with respect to f and S_e is given by

$$\begin{aligned}
L^{(fS_e)} = & \sum_k \left[\frac{-S}{(SD_k + S_e)^2} D_k^{(f)} \right] + S_e^{-1} \left[-\sum_k a_k^{(fS_e)} \frac{\boldsymbol{\Phi}^T \mathbf{D}_k \boldsymbol{\Phi}}{\|\boldsymbol{\Phi}\|^2} - \sum_k 2a_k^{(S_e)} (b_{Rk}^{(f)} b_{Rk} + b_{Ik}^{(f)} b_{Ik}) \right. \\
& - \sum_k a_k^{(fS_e)} (b_{Rk}^2 + b_{Ik}^2) + 2 \frac{\boldsymbol{\Phi}^T}{\|\boldsymbol{\Phi}\|} \sum_k a_k^{(fS_e)} (b_{Rk} \operatorname{Re} \mathcal{F}_k + b_{Ik} \operatorname{Im} \mathcal{F}_k) \\
& + 2 \frac{\boldsymbol{\Phi}^T}{\|\boldsymbol{\Phi}\|} \sum_k a_k^{(S_e)} (b_{Rk}^{(f)} \operatorname{Re} \mathcal{F}_k + b_{Ik}^{(f)} \operatorname{Im} \mathcal{F}_k) \left. \right] - S_e^{-2} \left[-\sum_k a_k^{(f)} \frac{\boldsymbol{\Phi}^T \mathbf{D}_k \boldsymbol{\Phi}}{\|\boldsymbol{\Phi}\|^2} \right. \\
& + \sum_k 2(1-a_k)(b_{Rk}^{(f)} b_{Rk} + b_{Ik}^{(f)} b_{Ik}) - \sum_k a_k^{(f)} (b_{Rk}^2 + b_{Ik}^2) \\
& \left. + 2 \frac{\boldsymbol{\Phi}^T}{\|\boldsymbol{\Phi}\|} \sum_k a_k^{(f)} (b_{Rk} \operatorname{Re} \mathcal{F}_k + b_{Ik} \operatorname{Im} \mathcal{F}_k) - 2 \frac{\boldsymbol{\Phi}^T}{\|\boldsymbol{\Phi}\|} \sum_k (1-a_k)(b_{Rk}^{(f)} \operatorname{Re} \mathcal{F}_k + b_{Ik}^{(f)} \operatorname{Im} \mathcal{F}_k) \right]
\end{aligned} \tag{14}$$

The expression of $L^{(\zeta S_e)}$ is similar to $L^{(fS_e)}$.

The cross derivative of L with respect to f and u is given by

$$\begin{aligned}
L^{(fu)} = & S_e^{-1} \left[\sum_k 2(1-a_k)(b_{Rk}^{(fu)} b_{Rk} + b_{Ik}^{(fu)} b_{Ik} + b_{Rk}^{(f)} b_{Rk}^{(u)} + b_{Ik}^{(f)} b_{Ik}^{(u)}) \right. \\
& - \sum_k 2a_k^{(f)} (b_{Rk} b_{Rk}^{(u)} + b_{Ik} b_{Ik}^{(u)}) + 2 \frac{\boldsymbol{\Phi}^T}{\|\boldsymbol{\Phi}\|} \sum_k a_k^{(f)} (b_{Rk}^{(u)} \operatorname{Re} \mathcal{F}_k + b_{Ik}^{(u)} \operatorname{Im} \mathcal{F}_k) \\
& \left. - 2 \frac{\boldsymbol{\Phi}^T}{\|\boldsymbol{\Phi}\|} \sum_k (1-a_k)(b_{Rk}^{(fu)} \operatorname{Re} \mathcal{F}_k + b_{Ik}^{(fu)} \operatorname{Im} \mathcal{F}_k) \right]
\end{aligned} \tag{15}$$

The expression of $L^{(\zeta u)}$ is similar to $L^{(fu)}$.

The cross derivative of L with respect to f and v is given by

$$\begin{aligned}
L^{(fv)} = & S_e^{-1} \left[\sum_k 2(1-a_k)(b_{Rk}^{(fv)} b_{Rk} + b_{Ik}^{(fv)} b_{Ik} + b_{Rk}^{(f)} b_{Rk}^{(v)} + b_{Ik}^{(f)} b_{Ik}^{(v)}) \right. \\
& - \sum_k 2a_k^{(f)} (b_{Rk} b_{Rk}^{(v)} + b_{Ik} b_{Ik}^{(v)}) + 2 \frac{\boldsymbol{\Phi}^T}{\|\boldsymbol{\Phi}\|} \sum_k a_k^{(f)} (b_{Rk}^{(v)} \operatorname{Re} \mathcal{F}_k + b_{Ik}^{(v)} \operatorname{Im} \mathcal{F}_k) \\
& \left. - 2 \frac{\boldsymbol{\Phi}^T}{\|\boldsymbol{\Phi}\|} \sum_k (1-a_k)(b_{Rk}^{(fv)} \operatorname{Re} \mathcal{F}_k + b_{Ik}^{(fv)} \operatorname{Im} \mathcal{F}_k) \right]
\end{aligned} \tag{16}$$

The expression of $L^{(\zeta v)}$ is similar to $L^{(fv)}$.

The cross derivative of L with respect to S and u is given by

$$L^{(Su)} = S_e^{-1} [-\sum_k 2a_k^{(S)} (b_{Rk} b_{Rk}^{(u)} + b_{Ik} b_{Ik}^{(u)}) + 2 \frac{\boldsymbol{\Phi}^T}{\|\boldsymbol{\Phi}\|} \sum_k a_k^{(S)} (b_{Rk}^{(u)} \text{Re } \mathcal{F}_k + b_{Ik}^{(u)} \text{Im } \mathcal{F}_k)] \quad (17)$$

The expression of $L^{(Sv)}$ is similar to $L^{(Su)}$.

The cross derivative of L with respect to S_e and u is given by

$$\begin{aligned} L^{(S_e u)} &= S_e^{-1} [-\sum_k 2a_k^{(S_e)} (b_{Rk} b_{Rk}^{(u)} + b_{Ik} b_{Ik}^{(u)}) + 2 \frac{\boldsymbol{\Phi}^T}{\|\boldsymbol{\Phi}\|} \sum_k a_k^{(S_e)} (b_{Rk}^{(u)} \text{Re } \mathcal{F}_k + b_{Ik}^{(u)} \text{Im } \mathcal{F}_k)] \\ &\quad - S_e^{-2} [\sum_k 2(1-a_k) (b_{Rk} b_{Rk}^{(u)} + b_{Ik} b_{Ik}^{(u)}) - 2 \frac{\boldsymbol{\Phi}^T}{\|\boldsymbol{\Phi}\|} \sum_k (1-a_k) (b_{Rk}^{(u)} \text{Re } \mathcal{F}_k + b_{Ik}^{(u)} \text{Im } \mathcal{F}_k)] \end{aligned} \quad (18)$$

The expression of $L^{(S_e v)}$ is similar to $L^{(S_e u)}$.

The cross derivative of L with respect to S_e and S is given by

$$\begin{aligned} L^{(SS_e)} &= -\sum_k [\frac{D_k}{(SD_k + S_e)^2}] + S_e^{-1} [-\sum_k a_k^{(SS_e)} \frac{\boldsymbol{\Phi}^T \mathbf{D}_k \boldsymbol{\Phi}}{\|\boldsymbol{\Phi}\|^2} - \sum_k a_k^{(SS_e)} (b_{Rk}^2 + b_{Ik}^2) \\ &\quad + 2 \frac{\boldsymbol{\Phi}^T}{\|\boldsymbol{\Phi}\|} \sum_k a_k^{(SS_e)} (b_{Rk} \text{Re } \mathcal{F}_k + b_{Ik} \text{Im } \mathcal{F}_k)] - S_e^{-2} [-\sum_k a_k^{(S)} \frac{\boldsymbol{\Phi}^T \mathbf{D}_k \boldsymbol{\Phi}}{\|\boldsymbol{\Phi}\|^2} - \sum_k a_k^{(S)} (b_{Rk}^2 + b_{Ik}^2) \\ &\quad + 2 \frac{\boldsymbol{\Phi}^T}{\|\boldsymbol{\Phi}\|} \sum_k a_k^{(S)} (b_{Rk} \text{Re } \mathcal{F}_k + b_{Ik} \text{Im } \mathcal{F}_k)] \end{aligned} \quad (19)$$

The cross derivative of L with respect to f and $\boldsymbol{\Phi}$ is given by

$$\begin{aligned} L^{(f\boldsymbol{\Phi})} &= 2S_e^{-1} [-(\frac{\mathbf{I}_n}{\|\boldsymbol{\Phi}\|^2} - \frac{\boldsymbol{\Phi}\boldsymbol{\Phi}^T}{\|\boldsymbol{\Phi}\|^4}) \sum_k a_k^{(f)} \mathbf{D}_k \boldsymbol{\Phi} + (\frac{\mathbf{I}_n}{\|\boldsymbol{\Phi}\|} - \frac{\boldsymbol{\Phi}\boldsymbol{\Phi}^T}{\|\boldsymbol{\Phi}\|^3}) \sum_k a_k^{(f)} (b_{Rk} \text{Re } \mathcal{F}_k + b_{Ik} \text{Im } \mathcal{F}_k) \\ &\quad - (\frac{\mathbf{I}_n}{\|\boldsymbol{\Phi}\|} - \frac{\boldsymbol{\Phi}\boldsymbol{\Phi}^T}{\|\boldsymbol{\Phi}\|^3}) \sum_k (1-a_k) (b_{Rk}^{(f)} \text{Re } \mathcal{F}_k + b_{Ik}^{(f)} \text{Im } \mathcal{F}_k)] \end{aligned} \quad (20)$$

The expression of $L^{(\zeta\boldsymbol{\Phi})}$ is similar to $L^{(f\boldsymbol{\Phi})}$.

The cross derivative of L with respect to S and $\boldsymbol{\Phi}$ is given by

$$L^{(S\Phi)} = 2S_e^{-1}[-(\frac{\mathbf{I}_n}{\|\Phi\|^2} - \frac{\Phi\Phi^T}{\|\Phi\|^4})\sum_k a_k^{(S)}\mathbf{D}_k\Phi + (\frac{\mathbf{I}_n}{\|\Phi\|} - \frac{\Phi\Phi^T}{\|\Phi\|^3})\sum_k a_k^{(S)}(b_{Rk}\text{Re}\mathcal{F}_k + b_{Ik}\text{Im}\mathcal{F}_k)] \quad (21)$$

The cross derivative of L with respect to S_e and Φ is given by

$$\begin{aligned} L^{(S_e\Phi)} &= 2S_e^{-1}[-(\frac{\mathbf{I}_n}{\|\Phi\|^2} - \frac{\Phi\Phi^T}{\|\Phi\|^4})\sum_k a_k^{(S_e)}\mathbf{D}_k\Phi + (\frac{\mathbf{I}_n}{\|\Phi\|} - \frac{\Phi\Phi^T}{\|\Phi\|^3})\sum_k a_k^{(S_e)}(b_{Rk}\text{Re}\mathcal{F}_k + b_{Ik}\text{Im}\mathcal{F}_k)] \\ &+ 2S_e^{-2}[(\frac{\mathbf{I}_n}{\|\Phi\|^2} - \frac{\Phi\Phi^T}{\|\Phi\|^4})\sum_k a_k\mathbf{D}_k\Phi + (\frac{\mathbf{I}_n}{\|\Phi\|} - \frac{\Phi\Phi^T}{\|\Phi\|^3})\sum_k (1-a_k)(b_{Rk}\text{Re}\mathcal{F}_k + b_{Ik}\text{Im}\mathcal{F}_k)] \end{aligned} \quad (22)$$

The cross derivative of L with respect to u and Φ is given by

$$L^{(u\Phi)} = 2S_e^{-1}[(\frac{\mathbf{I}_n}{\|\Phi\|} - \frac{\Phi\Phi^T}{\|\Phi\|^3})\sum_k (a_k - 1)(b_{Rk}^{(u)}\text{Re}\mathcal{F}_k + b_{Ik}^{(u)}\text{Im}\mathcal{F}_k)] \quad (23)$$

The expression of $L^{(v\Phi)}$ is similar to $L^{(u\Phi)}$.

4. Hessian for general multiple modes (ignoring ambient vibration)

For general multiple modes (ignoring ambient vibration), the NLLF is given by (66) of the companion paper [1] (in terms of normalized mode shapes).

$$L(\Theta', S_e) = nN_f \ln \pi + nN_f \ln S_e + S_e^{-1} J(\Theta') \quad (24)$$

where

$$J(\Theta') = (\overline{\Phi} :)^T \mathbf{Q}_1(\{f_i, \zeta_i, u_i, v_i\})(\overline{\Phi} :) - 2(\overline{\Phi} :)^T \mathbf{Q}_2(\{f_i, \zeta_i, u_i, v_i\}) + \sum_k \mathcal{F}_k^* \mathcal{F}_k \quad (25)$$

and $(\overline{\Phi} :) \in \mathbf{R}^{mn}$ denotes the ‘vectorization’ of $\overline{\Phi} = [\overline{\Phi}(1), \dots, \overline{\Phi}(m)]$, formed by stacking column-wise its columns, i.e.,

$$(\overline{\Phi} :) = \begin{bmatrix} \overline{\Phi}(1) \\ \vdots \\ \overline{\Phi}(m) \end{bmatrix} \quad (26)$$

and $\mathbf{Q}_1 \in \mathbf{R}^{mn \times mn}$ is given by

$$\mathbf{Q}_1(\{f_i, \zeta_i, u_i, v_i\}) = [\sum_k \text{Re}(\mathbf{b}_k^* \mathbf{b}_k)] \otimes \mathbf{I}_n \quad (27)$$

and $\mathbf{Q}_2 \in R^{mn}$ is given by

$$\mathbf{Q}_2(\{f_i, \zeta_i, u_i, v_i\}) = \sum_k \text{Re}(\mathbf{b}_k^* \otimes \mathcal{F}_k) \quad (28)$$

where

$$\mathbf{b}_k = [b_{1k}, \dots, b_{mk}] \quad (29)$$

and $b_{ik} (i = 1, \dots, m)$ is given by

$$b_{ik} = \sqrt{\frac{2\Delta t}{N}} \sum_{j=1}^N [u_i g_{1i}(t_j) + v_i g_{2i}(t_j)] \exp[-2\pi i \frac{(k-1)(j-1)}{N}] \quad (k = 1, \dots, N) \quad (30)$$

where $g_{1i}(t_j)$ and $g_{2i}(t_j)$ are given by

$$g_{1i}(t_j) = e^{-\zeta_i \omega_{di} t_j} (\cos \omega_{di} t_j + \frac{\zeta_i}{\sqrt{1-\zeta_i^2}} \sin \omega_{di} t_j) \quad (31)$$

$$g_{2i}(t_j) = \frac{e^{-\zeta_i \omega_{di} t_j}}{\omega_{di}} \sin \omega_{di} t_j \quad (32)$$

The derivatives with respect to $\{f_i, \zeta_i, u_i, v_i : i = 1, \dots, m\}$ and S_e are presented next. Due to the complication of the posterior uncertainty of mode shape, independent discussion will be given later.

4.1. Derivatives of $\{f_i, \zeta_i, u_i, v_i : i = 1, \dots, m\}$ and S_e

Recall that $\boldsymbol{\theta}'$ is given by

$$\boldsymbol{\theta}' = \{f_i, \zeta_i, u_i, v_i \in R : i = 1, \dots, m; \overline{\boldsymbol{\Phi}} \in R^{n \times m}\} \quad (33)$$

As the prediction error S_e has a different role from other parameters, it is separately treated.

Let the variable z represent any one of the parameters in $\boldsymbol{\theta}'$. The cross derivative of the NLLF with respect to z and S_e comes only from the third term of the right hand side (RHS) of (24). This gives

$$L^{(zS_e)} = -S_e^{-2} J^{(z)} \quad (34)$$

At the MPV of z , $J^{(z)} = 0$ and so $L^{(zS_e)} = 0$. This means that the cross derivatives of NLLF with respect to $\boldsymbol{\theta}'$ and S_e are equal to zero. Thus \mathbf{H}_L is a block-diagonal $(4m + mn + 1)$ -square matrix with the following structure:

$$\mathbf{H}_L = \begin{bmatrix} S_e^{-1} \mathbf{H}_J & \\ & L^{(S_e S_e)} \end{bmatrix} \quad (35)$$

where $\mathbf{H}_J \in R^{(4m+mn) \times (4m+mn)}$ is the Hessian of $J(\boldsymbol{\theta}')$. The corresponding posterior covariance matrix \mathbf{C} is then also a block-diagonal matrix given by

$$\mathbf{C} = \mathbf{H}_L^{-1} = \begin{bmatrix} S_e \mathbf{H}_J^{-1} & \\ & L^{(S_e S_e)^{-1}} \end{bmatrix} \quad (36)$$

The posterior covariance matrix of $\boldsymbol{\theta}'$ and the variance of S_e can thus be evaluated separately. The latter is simply equal to the reciprocal of $L^{(S_e S_e)}$:

$$\sigma_{S_e}^2 = (L^{(S_e S_e)})^{-1} = \frac{\hat{S}_e^2}{nN_f} \quad (37)$$

where \hat{S}_e is the MPV of S_e ; n is the number of measured degree of freedoms (dofs); N_f is the number of frequency components in the selected frequency band. It remains to calculate the Hessian of J with respect to $\boldsymbol{\theta}'$, i.e., \mathbf{H}_J .

The posterior uncertainties of $\{f_i, \zeta_i, u_i, v_i\}$ are all scalars, but the mode shape is a matrix, and so it is convenient to separate $\boldsymbol{\theta}'$ into two groups of parameters $\{f_i, \zeta_i, u_i, v_i\}$ and $(\overline{\boldsymbol{\Phi}})$. The first term on the RHS of $J(\boldsymbol{\theta}')$ in (25) is written more explicitly as

$$(\overline{\Phi} :)^T \mathbf{Q}_1(\{f_i, \zeta_i, u_i, v_i\})(\overline{\Phi} :) = \sum_{i,j=1}^m \sum_k \overline{\Phi}(i)^T [\text{Re}(\mathbf{B}_k(i, j)) \otimes \mathbf{I}_n] \overline{\Phi}(j) = \sum_k \left[\left(\sum_k \text{Re} \mathbf{B}_k \right) \bullet (\overline{\Phi}^T \overline{\Phi}) \right] \quad (38)$$

where ‘ \bullet ’ denotes an entry-by-entry multiplication of the subject matrices; $\Sigma[\cdot]$ denotes the sum of all entries in the argument matrix; and

$$\mathbf{B}_k = \mathbf{b}_k^* \mathbf{b}_k \in \mathbb{C}^{m \times m} \quad (39)$$

The second term on the RHS of $J(\boldsymbol{\theta}')$ in (25) is written as

$$-2(\overline{\Phi} :)^T \mathbf{Q}_2(\{f_i, \zeta_i, u_i, v_i\}) = -2 \sum_{i=1}^m \sum_k \overline{\Phi}(i)^T \text{Re}(b_{ik}^* \mathcal{F}_k) = -2 \sum_{i=1}^m \sum_k \text{Re}(b_{ik} \mathcal{F}_k^*) \overline{\Phi}(i) \quad (40)$$

Substituting (38) and (40) into (25), it can be re-written as

$$J(\boldsymbol{\theta}') = \sum_k \left[\left(\sum_k \text{Re} \mathbf{B}_k \right) \bullet (\overline{\Phi}^T \overline{\Phi}) \right] - 2 \sum_{i=1}^m \sum_k \text{Re}(b_{ik} \mathcal{F}_k^*) \overline{\Phi}(i) + \sum_k \mathcal{F}_k^* \mathcal{F}_k \quad (41)$$

Let z_i denote f_i, ζ_i, u_i or v_i , $i = 1, \dots, m$. The first derivative of $J(\boldsymbol{\theta}')$ is given by

$$J^{(z_i)} = \sum_k \left[\left(\sum_k \text{Re} \mathbf{B}_k^{(z_i)} \right) \bullet (\overline{\Phi}^T \overline{\Phi}) \right] - 2 \sum_k \text{Re}(b_{ik}^{(z_i)} \mathcal{F}_k^*) \overline{\Phi}(i) \quad (42)$$

The second derivative of $J(\boldsymbol{\theta}')$ is given by

$$J^{(z_i z_j)} = \sum_k \left[\left(\sum_k \text{Re} \mathbf{B}_k^{(z_i z_j)} \right) \bullet (\overline{\Phi}^T \overline{\Phi}) \right] - 2 \delta_{ij} \sum_k \text{Re}(b_{ik}^{(z_i z_j)} \mathcal{F}_k^*) \overline{\Phi}(i) \quad (43)$$

where δ_{ij} is the Dirac Delta function, equal to 1 if $i = j$ and zero otherwise.

Note that \mathbf{B}_k in (39) is a Hermitian matrix, whose first two derivatives are given by

$$\mathbf{B}_k^{(z_i)} = b_{ik}^{(z_i)*} \mathbf{e}_i \mathbf{b}_k + b_{ik}^{(z_i)} \mathbf{b}_k^* \mathbf{e}_i^T \quad (44)$$

$$\mathbf{B}_k^{(z_i z_j)} = [b_{ik}^{(z_i)*} b_{jk}^{(z_j)} \mathbf{E}_{ij} + b_{ik}^{(z_i)} b_{jk}^{(z_j)*} \mathbf{E}_{ji}] + \delta_{ij} [b_{ik}^{(z_i z_j)*} \mathbf{E}_i^T \text{diag}(\mathbf{b}_k) + b_{ik}^{(z_i z_j)} \text{diag}(\mathbf{b}_k^*) \mathbf{E}_i] \quad (45)$$

where $\mathbf{e}_i \in R^m$ denotes a column vector with the i -th entry being the only non-zero entry equal to unity; $\mathbf{E}_{ij} \in R^{m \times m}$ denotes a matrix with the (i, j) -entry being the only non-zero entry equal to 1; $\mathbf{E}_i \in R^{m \times m}$ denotes a matrix with the i -th column being the only non-zero column whose entries are all equal to 1; and $\text{diag}(\cdot)$ denotes a diagonal matrix formed by the argument vector.

4.2. Derivatives of $\overline{\Phi}$

The cross derivative between z_i and $\Phi_{r_1 s_1}$ (the (r_1, s_1) -entry of Φ , where $r_1 = 1, \dots, n$ and $s_1 = 1, \dots, m$) based on (41) is equal to

$$J^{(z_i \Phi_{r_1 s_1})} = \sum_k \left[\left(\sum_k \text{Re} \mathbf{B}_k^{(z_i)} \right) \bullet (\overline{\Phi}^T \overline{\Phi})^{(\Phi_{r_1 s_1})} \right] - 2\delta_{is_1} \sum_k \text{Re}(b_{ik}^{(z_i)} F_k^*) \overline{\Phi}(i)^{(\Phi_{r_1 s_1})} \quad (46)$$

and its second derivative with respect to the components of Φ is

$$J^{(\Phi_{r_1 s_1} \Phi_{r_2 s_2})} = \sum_k \left[\left(\sum_k \text{Re} \mathbf{B}_k \right) \bullet (\overline{\Phi}^T \overline{\Phi})^{(\Phi_{r_1 s_1} \Phi_{r_2 s_2})} \right] - 2\delta_{s_1 s_2} \sum_k \text{Re}(b_{s_1 k} F_k^*) \overline{\Phi}(s_1)^{(\Phi_{r_1 s_1} \Phi_{r_2 s_2})} \quad (47)$$

where the derivatives of $\overline{\Phi}^T \overline{\Phi}$ are given by [5]

$$(\overline{\Phi}^T \overline{\Phi})^{(\Phi_{r_1 s_1})} = \overline{\Phi}^{(\Phi_{r_1 s_1})T} \overline{\Phi} + \overline{\Phi}^T \overline{\Phi}^{(\Phi_{r_1 s_1})} \quad (48)$$

$$(\overline{\Phi}^T \overline{\Phi})^{(\Phi_{r_1 s_1} \Phi_{r_2 s_2})} = \overline{\Phi}^{(\Phi_{r_1 s_1} \Phi_{r_2 s_2})T} \overline{\Phi} + \overline{\Phi}^{(\Phi_{r_1 s_1})T} \overline{\Phi}^{(\Phi_{r_2 s_2})} + \overline{\Phi}^{(\Phi_{r_2 s_2})T} \overline{\Phi}^{(\Phi_{r_1 s_1})} + \overline{\Phi}^T \overline{\Phi}^{(\Phi_{r_1 s_1} \Phi_{r_2 s_2})} \quad (49)$$

where $\overline{\Phi}^{(\Phi_{r_1 s_1})}$ is a n -by- m matrix with the s_1 -th column being the only non-zero column equal to

$$\overline{\Phi}(s_1)^{(\Phi_{r_1 s_1})} = \|\Phi(s_1)\|^{-1} [\mathbf{e}_{r_1} - \overline{\Phi}_{r_1 s_1} \overline{\Phi}(s_1)] \quad (50)$$

where $\overline{\Phi}_{r_1 s_1}$ denotes the (r_1, s_1) entry of $\overline{\Phi}$. The cross derivative of the mode shape matrix between mode shape components of different modes is zero, i.e.,

$$\overline{\Phi}^{(\Phi_{r_1 s_1} \Phi_{r_2 s_2})} = \mathbf{0}_{n \times m} \text{ for } s_1 \neq s_2 \quad (51)$$

For the same mode s_1 , $\overline{\Phi}^{(\phi_{r_1 s_1} \phi_{r_2 s_1})}$ is a n -by- m matrix with the s_1 -th column being the only non-zero column equal to

$$\overline{\Phi}(s_1)^{(\phi_{r_1 s_1} \phi_{r_2 s_1})} = \|\Phi(s_1)\|^{-2} [(3\overline{\Phi}_{r_1 s_1} \overline{\Phi}_{r_2 s_1} - \delta_{r_1 r_2}) \overline{\Phi}(s_1) - \overline{\Phi}_{r_2 s_1} \mathbf{e}_{r_1} - \overline{\Phi}_{r_1 s_1} \mathbf{e}_{r_2}] \quad (52)$$

5. Verification with synthetic data

Consider a 5-storied shear frame with floor plan measuring $0.5m \times 0.5m$. Assuming rigid floor diaphragm, the shear frame has a uniform inter-story stiffness of $100 kN/m$ in x direction, $125 kN/m$ in y direction. Each floor has a mass of $50 kg$ and moment of inertia of $2.083 kg \cdot m^2$. It is targeted to obtain modal properties in the translational and torsional directions of this structure. The fundamental natural frequency is calculated to be $2.03 Hz$. Classical damping is assumed with a damping ratio of 1% in all modes. Biaxial horizontal acceleration measurement with a sampling rate of $100Hz$ is assumed to be available at the locations shown in Figure 1. Therefore, there are total 60 dofs measured with 12 dofs for each floor.

5.1. Nominal case

We first consider a nominal case, based on which further discussions are expanded later. The frame is always subjected to ambient excitation at all the floor levels modeled by independent and identically distributed (i.i.d.) Gaussian white noise in the x , y and torsional directions, with a one-sided root power spectral density (PSD) of 3×10^{-4} , $3 \times 10^{-4} N/\sqrt{Hz}$ and $0.375 \times 10^{-4} Nm/\sqrt{Hz}$, respectively. An impulse is given to the fifth floor of this structure to produce free vibration with initial displacement and velocity of fifteen modes shown in Table 1. Note that in the simulation, the responses at the 12 dofs on each floor were calculated from the simulated responses from two translational and one torsional dofs at the center of each floor based on the rigid floor assumption. The initial conditions of the free vibration response depend on the norm of the mode shape. In this study, they are calculated by setting the norms of the mode shapes contained the 15 dofs at the center of all 5 floors equal to unity.

Acceleration data of 60 seconds duration is generated. The measured acceleration is contaminated by measurement noise modeled by i.i.d. Gaussian white noise with a root spectral

density of $3 \mu g / \sqrt{Hz}$ in every channel. According to Parseval equality, the integral (or area) of the spectral density over all frequencies is equal to the variance. Therefore, the standard derivation of the measurement noise is equal to $\sqrt{S_e f_s / 2}$, where S_e is the PSD of prediction error and f_s is the sampling frequency. The time history of data is shown in Figure 2. Figure 3 shows the root PSD and root singular value (SV) spectra of the data. The SV spectra is used for locating the initial guess of the natural frequency and the frequency band for modal identification, where the number, the dot and the line denote the mode number, the initial guess of natural frequency, and the selected frequency band, respectively. Modal identification is performed for each band separately.

5.1.1 Well-separated modes (Method I)

Figure 4 summarizes the modal properties (MPV) of Modes 1 to 6. The dots on the 1st to 5th floors show the measured locations, while those on the ground floor are always fixed. Table 2 and Table 3 show the ‘exact’ modal parameters used in generating the data and the MPV of the identified modal parameters with the associated posterior uncertainty, respectively. The MPVs are close to their exact values in a manner consistent with their posterior coefficient of variation (c.o.v.= standard derivation / MPV). For the PSD of prediction error S_e , the exact values in the synthetic example only include the channel noise in the ambient conditions. There is an apparent bias in the identified values because they include smearing effects from unaccounted modes. A similar effect may occur in the initial conditions. The identified values of initial modal acceleration u and its derivative v are generally in the same order of magnitude with the exact ones.

The last two columns in Table 3 show the Modal Assurance Criteria (MAC) between the identified and exact mode shapes and the quantity 1-EMAC (Expected MAC) to describe the posterior uncertainty of mode shape [14]. The closer the value of EMAC to unity, the smaller the posterior uncertainty will be. The EMAC values in all the modes are also quite close to 1, which indicates that the posterior uncertainties of the identified mode shapes are very small. Overall, it is concluded that the posterior uncertainties of the natural frequency, damping ratio and mode shape are very small, even if only 60 seconds data is used. Figure 5 shows the root PSD of

measured data and theoretical root PSD corresponding to the MPV, which shows a good agreement.

5.1.2 General multiple modes (Ignoring ambient vibration) (Method II)

As mentioned before, Method II that ignores ambient vibration is applicable for general multiple modes. In this verification, the first three modes are included in the same band for modal identification. For consistency, in this band, its lower and upper values are equal to the lower value of the frequency band of Mode 1 and the upper value of the frequency band of Mode 3 in Method I, respectively. Modes 4 and 5 are also included in the same band. The way to select the lower and upper values of the band is similar, i.e., they are equal to the lower value of the frequency band of Mode 4 and the upper value of the frequency band of Mode 5 in Method I, respectively. Mode 6 is identified separately with the same band as the case in Method I. Table 4 shows the MPV of the identified modal parameters and their posterior uncertainty. It should be noted that, although the MPVs in Table 4 are similar to those in Table 3, the same is not true for the c.o.v.s. In particular, the c.o.v.s in Table 4 are generally smaller than those in Table 3. This difference is due to the different assumptions made in the identification models of two methods. This demonstrates the importance of the assumption used and the interpretation of posterior uncertainty results. In the present case, those c.o.v.s in Table 3 are a better reflection of reality because there is less modeling error. Comparing the PSD of prediction error in Table 3 and Table 4 with the exact values in Table 2, the results of the first five modes identified using Method II are more close to the exact values. This is because the modal identification process was divided into two parts in Method II (i.e., the first three modes were in one frequency band and identified simultaneously; the fourth and fifth modes were in another frequency band and identified simultaneously) while all modes were identified individually in Method I. When two or three modes are identified simultaneously, the effects of uncounted modes will be reduced, which leads to the reduction in the PSD of prediction error during modal identification. This argument is supported by the result from the sixth identified mode, which was identified separately in both Methods I and II and the PSD of prediction error were in the same order of magnitude in both methods. Figure 6 shows the root PSD of measured data and the theoretical root PSD corresponding to the MPV, which also show a good agreement.

5.2. Parametric study of Method II

In the process of vibration test and modal identification, there are lots of factors that may influence the accuracy of the data collected, and consequently the modal identification accuracy. Since in Method II, the ambient vibration response is modeled to be prediction error, it is worth investigating the effects of measurement noise and ambient vibration levels on the identified modal parameters using synthetic data.

5.2.1 Effect of measurement noise

To investigate the effect of the measurement noise and check the model considered, six noise levels are considered from lower to higher in terms of their PSD value: $9 \times 10^{-12} \text{ g}^2/\text{Hz}$, $90 \times 10^{-12} \text{ g}^2/\text{Hz}$, $450 \times 10^{-12} \text{ g}^2/\text{Hz}$, $900 \times 10^{-12} \text{ g}^2/\text{Hz}$, $1800 \times 10^{-12} \text{ g}^2/\text{Hz}$, and $4500 \times 10^{-12} \text{ g}^2/\text{Hz}$. The first level corresponds to the nominal case that has been investigated in Section 5.1.

When studying the effect of noise level, in order to remove the influence of the unmodeled ambient vibration part, no ambient vibration response is simulated in the data used. The effect of ambient vibration will be discussed separately in Section 5.2.2. Figure 7 summarizes the results for different channel noise levels. In the figure, the identification result is shown with a dot at the MPV and an error bar shows the \pm two posterior standard deviations. The dashed line denotes the exact values of the corresponding identified modal parameters. Although the identified MPVs of higher noise have a lower accuracy than the typical case, they are relatively stable and close to their exact values. The main difference lies in the posterior uncertainty. The posterior c.o.v.s of natural frequencies and damping ratios grow gradually for all the six modes with the noise level. There is no significant bias observed in the figure even when the noise is relatively high, in the sense that the corresponding posterior probability density function implied by the error bars covers the exact value. This indicates that the consideration of the prediction error in the proposed theory is capable of addressing the channel noise effect.

5.2.2 Effect of ambient vibration

Recall from the theory of Method II that ambient vibration response is not explicitly modeled in the formulation but is absorbed in the prediction error, for which only a simple channel noise model is adopted. The effect of ambient vibration on the modal identification results may be

significant and is investigated in this section. In the synthetic data the loading always consists of the ambient force, and thus modeling error already exists in the nominal case. To further investigate the ambient vibration effect, different ambient load levels in terms of a one-sided root spectral density of normal case multiplied by 0.0001, 0.001, 0.01, 0.1, 1 and 2 separately are considered.

Figure 8 summarizes the results for different ambient vibration levels. When the ambient excitation increases, the posterior c.o.v. only changes slightly. Some bias is seen when the ambient excitation is large, as reflected by the systematic departure of the error bar from the dashed line in the figure. Here, the dashed line is the exact value for reference. The apparent bias can be attributed to the fact that the effect of the ambient load is not explicitly accounted for in the identification model, but is only ‘gross-overed’ into the prediction error S_e .

6. Field applications

6.1 Tanjong Rhu Bridge

The first structure is the Tanjong Rhu suspension bridge as shown in Figure 9, which spans across Kallang River in Singapore. It is about 130m long with 80m main span and two 25m side spans, and 4m wide. Fourteen locations are measured with accelerometers and acceleration data are acquired at a sampling rate of 100 Hz. At the time of instrumentation, only four sensors were available. Six setups were then designed to cover all the locations of interest. Free vibration response is generated by human excitation, with two persons jumping on the bridge at near the natural frequency and at the locations where the mode shape component is large. Four modes are focused, i.e., VS1 and VS2 (the first two symmetric bending modes), VA1 (the first asymmetric bending mode), TS1 (the first torsional mode). The jumping excitation generally continued for about two minutes, after which, about 60 seconds structural response is recorded. The detailed field test and dynamic characteristics of the bridge have been previously presented [15].

Figure 10 shows a typical time history of the free acceleration response of Mode VA1. Figure 11 shows its root PSD and SV spectra. The results in terms of their MPV identified by the proposed method considering ambient vibration response (Method I) are summarized in Figure 12. The values in the subfigures denote the averaged natural frequency and damping ratio of all setups.

The thin and thick lines denote the undeformed and deformed shape of the bridge. The dots show the measured locations. Note that these mode shapes are assembled by a global least square method [16] using the individual mode shapes in different setups. The mode shapes identified by the method ignoring ambient vibration response (Method II) are similar, whose MAC values with the counterparts identified using Method I are over 0.99. Table 5 and Table 6 show the identified results of Setup 1 of all the four modes under investigation using Methods I and II, respectively. The properties in other setups are similar. Figure 13 shows the root PSD of measured data and the theoretical root PSD corresponding to the MPV using Method I, which shows a good agreement. The picture for Method II is similar.

Although the MPVs of modal parameters identified using Methods I and II are close to each other, the posterior uncertainties corresponding to Method I are obviously different from those in Method II. Again, this is because the two methods have different assumption about the prediction error. The model of Method I with ambient vibration response considered is a better one, although it is more complicated. However, this does not render Method II dispensable, because it can handle both closely-spaced and well-separated modes.

Figure 14 to Figure 17 show the identified natural frequencies and damping ratios (using Method I) corresponding to different setups of Modes 1 to 3, respectively. From the error bars, it is found that the modal parameters change with different setups, especially for the natural frequencies of VS1 and VA1. The results identified using the least square method mentioned in [15] are similar to those identified using proposed method. This may be because that the data in different setups were measured at different time. The properties of the bridge may have a little change during a whole day. The error bars only reflect the accuracy of the parameters in each setup but they do not necessarily predict the identification results in the next setup. These figures should be viewed with both a Bayesian and frequentist perspectives [17].

6.2 CityU bridge

The second subject structure is a concrete pedestrian bridge situated at the entrance of the City University of Hong Kong (CityU) as shown in Figure 18. It measures 55 *m* long by 12.8 *m* wide. The footbridge has three spans. In this study, only the second span of a 20 *m* segment is

instrumented. Figure 19 shows the detailed setup plan for the test. The number next to each sensor is the dof number. Only the vertical acceleration is measured at each location. Guralp CMG5T forced-balanced tri-axial accelerometers (only vertical channel used), indicated by circles, are used for Locations 1, 2, 3, 7, 9, 10. The remaining locations are measured with Kistler K8330 uniaxial accelerometers, indicated by squares. The Guralp sensor has a higher accuracy than the Kistler sensor, which means that it can provide higher s/n ratio data and be used in the locations where the structure response is relatively small or the noise level is relatively large.

The bridge is excited by an electro-magnetic shaker indicated by a triangle in Figure 19. That is, the shaker first generates the excitation to the bridge for a while, and then when it is turned off, the free vibration will occur. The frequency of the excitation can be changed by altering the frequency of input voltage by Labview software on a laptop. Note that in the beginning, a frequency sweep forced vibration test with more than ten exciting frequencies around each mode of interest is performed; in every frequency, sinusoidal excitation continues for about one minute, after which free vibration response is recorded. Digital data is acquired at a sampling rate of 2048Hz with 24 bit resolution. It is later decimated by 16 to a sample rate of 128 Hz for analysis and modal identification. Ten-minute of ambient data is first collected to roughly locate the dominant bands of the first few modes of interest. Modes are expected near 4.69 Hz (Mode 1), 6.67 Hz (Mode 2) and 10.96 Hz (Mode 3). Three groups of measured free vibration data corresponding to the three modes respectively are collected and used for modal identification.

Figure 20 shows the time history of Setup 1 for Mode 1, where free vibration response can be observed obviously. Figure 21 shows the root PSD and SV spectra, where the selected band of Mode 1 is indicated. Table 7 and Table 8 show the modal parameters corresponding to Setup 1 of three modes identified by Methods I and II, respectively. The parameters identified from other setups will be discussed later. The identified natural frequencies using the two methods are quite close to the values observed from the SV spectra. The damping ratios range between 0.8% to 2.4% with a c.o.v. of 1% to 32%. It is worth mentioning that the posterior uncertainties of the natural frequency, damping ratio and mode shape of Mode 3 are much bigger than those in Modes 1 and 2. This is because the free vibration response used to identify Mode 3 is not large,

as shown in Figure 22. The results of Method II (Table 8) for Mode 3 are potentially biased because it ignores the ambient vibration, which is not negligible here.

The mode shapes of the three modes identified using Method II from Setup 1 in terms of their MPV are shown in Figure 23. The first and third modes are bending modes in the vertical direction forming half sine and a whole sine wave, respectively. The second mode is a torsional mode. To further check the accuracy of modal parameters identified, Figure 24 shows the root PSD of measured data and the root PSD corresponding to the MPV. The mode shapes identified by Method I are almost the same with that in Method II with the MAC values over 0.99.

Recall that in each mode, more than 10 groups of free vibration data with different exciting frequency are recorded, based on which, the effect of exciting frequency is investigated. Figure 25 to Figure 27 show the natural frequencies and damping ratios identified by Method I corresponding to different excitation frequencies of Modes 1 to 3, respectively. It is seen that from the middle to both sides of the figures, the error bars tend to increase for either natural frequency or damping ratio. This is because the exciting frequencies near the middle of x axis are closer to the natural frequency of the subject mode; although the input forces all have similar magnitude. The free vibration responses when the shaker operates at near resonance are much larger than those off resonance.

7. Conclusions

In this work, a Bayesian formulation for modal identification using free vibration data has been presented, which can not only identify the most probable values (MPVs) of modal parameters of interest, but also analytically calculate the associated posterior uncertainties of the modal parameters. Two different cases, i.e., well-separated modes considering the ambient vibration response and general multiple (probably closely-spaced) modes ignoring the ambient vibration response, have been considered in the development of fast algorithms. Using free vibration data, Bayesian modal identification can be performed efficiently and practically even on site. Synthetic data and field data have been used to illustrate the proposed method. In the former data used, by modal identification using data with different noise and ambient vibration levels, it was discovered that the posterior uncertainties of modal parameters are influenced by the noise and

ambient vibration levels. When s/n ratio of the free vibration data is high, the posterior c.o.v. of modal parameters can be significantly smaller than their ambient counterparts. The posterior uncertainty calculated using Method I (considering ambient response) tends to be larger than that obtained using Method II (ambient response is modeled as noise), due to the different models used. Although the two methods can give reasonable results, they have different characteristics. Method I can work better in the case with significant ambient vibration since it is considered in the theory. Fast algorithm however has only been developed for well-separated modes because the mathematical structure of the likelihood function is much more complicated for multiple modes. By absorbing ambient vibration into the prediction error (therefore approximate), the mathematical structure in Method II is much simpler and so it allows fast algorithms to be developed in general for multiple modes.

Acknowledgements

The work described in this paper is partially supported by Fundamental Research Funds for the Central Universities, China (Grant No. 2014KJ040), a grant from the Research Grants Council of the Hong Kong Special Administrative Region, China (Project No. 9041758 (CityU 110012)) and Grant EGG10034 from the University of Liverpool.

Appendix

1. Derivatives of a_k

The quantity a_k is encountered frequently, whose derivatives with respect to $\{f, \zeta, S, S_e\}$ will be discussed. The general form of the derivatives with respect to any variables z_1 and z_2 can be presented firstly.

$$a_k^{(z_1)} = -a_k^2 (a_k^{-1})^{(z_1)} \quad (53)$$

$$a_k^{(z_1 z_2)} = 2a_k^3 (a_k^{-1})^{(z_1)} (a_k^{-1})^{(z_2)} - a_k^2 (a_k^{-1})^{(z_1 z_2)} \quad (54)$$

Base on the definition of general form, only the three terms, i.e., $(a_k^{-1})^{(z_1)}$, $(a_k^{-1})^{(z_2)}$ and $(a_k^{-1})^{(z_1 z_2)}$ need to be determined.

The first derivative of a_k^{-1} are given by

$$(a_k^{-1})^{(f)} = -\frac{S_e}{SD_k^2} D_k^{(f)}; (a_k^{-1})^{(\zeta)} = -\frac{S_e}{SD_k^2} D_k^{(\zeta)}; (a_k^{-1})^{(S_e)} = \frac{1}{SD_k}; (a_k^{-1})^{(S)} = -\frac{S_e}{S^2 D_k} \quad (55)$$

The second derivative of a_k^{-1} are given by

$$(a_k^{-1})^{(ff)} = \frac{2S_e(D_k^{(f)})^2}{SD_k^3} - \frac{S_e D_k^{(ff)}}{SD_k^2}; (a_k^{-1})^{(\zeta\zeta)} = \frac{2S_e(D_k^{(\zeta)})^2}{SD_k^3} - \frac{S_e D_k^{(\zeta\zeta)}}{SD_k^2}; (a_k^{-1})^{(S_e S_e)} = 0;$$

$$(a_k^{-1})^{(SS)} = 2\frac{S_e}{S^3 D_k} \quad (56)$$

The cross derivative of a_k^{-1} are given by

$$(a_k^{-1})^{(f\zeta)} = \frac{2S_e D_k^{(f)} D_k^{(\zeta)}}{SD_k^3} - \frac{S_e D_k^{(f\zeta)}}{SD_k^2}; (a_k^{-1})^{(fS_e)} = -\frac{1}{SD_k^2} D_k^{(f)}; (a_k^{-1})^{(\zeta S_e)} = -\frac{1}{SD_k^2} D_k^{(\zeta)};$$

$$(a_k^{-1})^{(fS)} = \frac{S_e}{S^2 D_k^2} D_k^{(f)}; (a_k^{-1})^{(\zeta S)} = \frac{S_e}{S^2 D_k^2} D_k^{(\zeta)}; (a_k^{-1})^{(S_e S)} = -\frac{1}{S^2 D_k} \quad (57)$$

where the derivatives of D_k can be found in [11].

2. Derivatives of b_{Rk} and b_{Ik}

Note that the derivatives of b_{Rk} and b_{Ik} are the k-th entries of the derivatives of b_R and b_I , respectively, which are presented as follows.

$$b_R^{(f)} = \text{Re}[\text{FFT}(ug_1^{(f)} + vg_2^{(f)})]; b_I^{(f)} = \text{Im}[\text{FFT}(ug_1^{(f)} + vg_2^{(f)})] \quad (58)$$

where $\text{Re}[\cdot]$ and $\text{Im}[\cdot]$ denote the real and imaginary parts, respectively; $\text{FFT}(\cdot)$ denotes the fast Fourier Transform (FFT) whose definition is similar to (2) in the companion paper. The expressions of $b_R^{(\zeta)}$ and $b_I^{(\zeta)}$ are similar to $b_R^{(f)}$ and $b_I^{(f)}$, respectively.

$$b_R^{(u)} = \text{Re}[\text{FFT}(g_1)]; b_I^{(u)} = \text{Im}[\text{FFT}(g_1)] \quad (59)$$

$$b_R^{(v)} = \text{Re}[\text{FFT}(g_2)]; b_I^{(v)} = \text{Im}[\text{FFT}(g_2)] \quad (60)$$

$$b_R^{(ff)} = \text{Re}[\text{FFT}(ug_1^{(ff)} + vg_2^{(ff)})]; b_I^{(ff)} = \text{Im}[\text{FFT}(ug_1^{(ff)} + vg_2^{(ff)})] \quad (61)$$

The expressions of $b_R^{(\zeta\zeta)}$ and $b_I^{(\zeta\zeta)}$ are similar to $b_R^{(ff)}$ and $b_I^{(ff)}$, respectively.

$$b_R^{(uu)} = \mathbf{0}; b_I^{(uu)} = \mathbf{0}; b_R^{(vv)} = \mathbf{0}; b_I^{(vv)} = \mathbf{0} \quad (62)$$

$$b_R^{(f\zeta)} = \text{Re}[\text{FFT}(ug_1^{(f\zeta)} + vg_2^{(f\zeta)})]; b_I^{(f\zeta)} = \text{Im}[\text{FFT}(ug_1^{(f\zeta)} + vg_2^{(f\zeta)})] \quad (63)$$

$$b_R^{(fu)} = \text{Re}[\text{FFT}(g_1^{(f)})]; b_I^{(fu)} = \text{Im}[\text{FFT}(g_1^{(f)})] \quad (64)$$

The expressions of $b_R^{(\zeta u)}$ and $b_I^{(\zeta u)}$ are similar to $b_R^{(fu)}$ and $b_I^{(fu)}$, respectively.

$$b_R^{(fv)} = \text{Re}[\text{FFT}(g_2^{(f)})]; b_I^{(fv)} = \text{Im}[\text{FFT}(g_2^{(f)})] \quad (65)$$

The expressions of $b_R^{(\zeta v)}$ and $b_I^{(\zeta v)}$ are similar to $b_R^{(fv)}$ and $b_I^{(fv)}$, respectively.

$$b_R^{(uv)} = \mathbf{0}; b_I^{(uv)} = \mathbf{0} \quad (66)$$

In the above expressions, the derivatives of the entries of g_1 and g_2 at time t_j ($j=1, \dots, N$) are given as follows.

The first derivative of $g_1(t_j)$ with respect to f is given by

$$g_1(t_j)^{(f)} = \frac{-2\pi t_j}{\sqrt{1-\zeta^2}} e^{-\zeta \omega t_j} \sin \omega_d t_j \quad (67)$$

The first derivative of $g_1(t_j)$ with respect to ζ is given by

$$g_1(t_j)^{(\zeta)} = \frac{e^{-\zeta\omega t_j}}{(1-\zeta^2)} \left(\frac{1}{\sqrt{1-\zeta^2}} \sin \omega_d t_j - \omega t_j \cos \omega_d t_j \right) \quad (68)$$

The second derivative of $g_1(t_j)$ with respect to f is given by

$$g_1(t_j)^{(ff)} = (2\pi t_j)^2 e^{-\zeta\omega t_j} \left(\frac{\zeta}{\sqrt{1-\zeta^2}} \sin \omega_d t_j - \cos \omega_d t_j \right) \quad (69)$$

The second derivative of $g_1(t_j)$ with respect to ζ is given by

$$g_1(t_j)^{(\zeta\zeta)} = e^{-\zeta\omega t_j} \left[-\frac{(\omega^2 t_j^2 \zeta + \omega t_j)(1-\zeta^2) - 3\zeta}{(1-\zeta^2)^2 \sqrt{1-\zeta^2}} \sin \omega_d t_j \right. \\ \left. + \frac{(1-\zeta^2)(\omega t_j)^2 - 3\omega t_j \zeta}{(1-\zeta^2)^2} \cos \omega_d t_j \right] \quad (70)$$

The cross derivative of $g_1(t_j)$ with respect to f and ζ is given by

$$g_1(t_j)^{(f\zeta)} = e^{-\zeta\omega t_j} \left[\frac{2\pi t_j(\omega t_j - \omega t_j \zeta^2 - \zeta)}{(1-\zeta^2)\sqrt{1-\zeta^2}} \sin \omega_d t_j + \frac{2\pi\omega t_j^2 \zeta}{(1-\zeta^2)} \cos \omega_d t_j \right] \quad (71)$$

The first derivative of $g_2(t_j)$ with respect to f is given by

$$g_2(t_j)^{(f)} = -\frac{\omega t_j \zeta + 1}{f} g_2(t_j) + \frac{2\pi t_j}{\omega} e^{-\zeta\omega t_j} \cos \omega_d t_j \quad (72)$$

The first derivative of $g_2(t_j)$ with respect to ζ is given by

$$g_2(t_j)^{(\zeta)} = \frac{\zeta - \omega t_j(1-\zeta^2)}{(1-\zeta^2)} g_2(t_j) - \frac{\omega t_j \zeta}{\omega_d \sqrt{1-\zeta^2}} e^{-\zeta\omega t_j} \cos \omega_d t_j \quad (73)$$

The second derivative of $g_2(t_j)$ with respect to f is given by

$$g_2(t_j)^{(ff)} = \frac{2(\omega t_j \zeta)^2 - (\omega t_j)^2 + 2\omega t_j \zeta + 2}{f^2} g_2(t_j) - \frac{2\omega t_j^2 \zeta + 2t_j}{f^2} e^{-\zeta\omega t_j} \cos \omega_d t_j \quad (74)$$

The second derivative of $g_2(t_j)$ with respect to ζ is given by

$$g_2(t_j)^{(\zeta\zeta)} = \frac{-3(\omega t_j \zeta)^2 + 2(\omega t_j \zeta^2)^2 - 2\omega t_j \zeta + 2\omega t_j \zeta^3 + (\omega t_j)^2 + 2\zeta^2 + 1}{(1 - \zeta^2)^2} g_2(t_j) + \frac{2t_j^2 \omega \zeta (1 - \zeta^2) - 2\zeta^2 t_j - t_j}{(1 - \zeta^2)^2} e^{-\zeta \omega t_j} \cos \omega_d t_j \quad (75)$$

The cross derivative of $g_2(t_j)$ with respect to f and ζ is given by

$$g_2(t_j)^{(f\zeta)} = \frac{-2(\omega t_j)^2 \zeta^3 + 2(\omega t_j)^2 \zeta - \omega t_j \zeta^2 - \zeta}{f(1 - \zeta^2)} g_2(t_j) + \frac{2\omega(t_j \zeta)^2 - \omega t_j^2 + t_j \zeta}{f(1 - \zeta^2)} e^{-\zeta \omega t_j} \cos \omega_d t_j \quad (76)$$

References

- [1] F.L. Zhang, Y.C. Ni, S. K. Au, H.F. Lam, Fast Bayesian approach for modal identification using free vibration data, Part I – Most probable value, Mechanical system and signal processing (2014).
- [2] R.T. Cox, The Algebra of Probable Inference, Johns Hopkins Press, Baltimore, 1961.
- [3] E. T. Jaynes, Probability theory: The logic of science, Cambridge University Press, UK. 2003.
- [4] J.L. Beck, Bayesian system identification based on probability logic, Structural Control and Health Monitoring 17(7) (2010) 825-847.
- [5] S.K. Au, Fast Bayesian ambient modal identification in the frequency domain, part II: posterior uncertainty, Mechanical Systems and Signal Processing 26 (2012) 76-90.
- [6] S.K. Au, F.L. Zhang, Y.C. Ni, Bayesian operational modal analysis: theory, computation, practice, Computers and Structures 126 (2013) 3-14.
- [7] C. Papadimitriou, J.L. Beck, L.S. Katafygiotis, Updating robust reliability using structural test data, Probabilistic Engineering Mechanics 16(2) (2001) 103-113.
- [8] J.M.W. Brownjohn, Ambient vibration studies for system identification of tall buildings, Earthquake Engineering and Structural Dynamics 32 (2003) 71-95.
- [9] B.F. Yan, A. Miyamoto, E. Bruhwiler, Wavelet transform-based modal parameter identification considering uncertainty, Journal of Sound and Vibration 291 (2006) 285 – 301.

- [10] S.K. Au and F.L Zhang, P. To, Field observations on modal properties of two super tall buildings under strong wind, *Journal of Wind Engineering & Industrial Aerodynamics* 101 (2012) 12-23.
- [11] S.K. Au, Fast Bayesian FFT method for ambient modal identification with separated modes, *Journal of Engineering Mechanics* 137(3) (2011) 214-226.
- [12] S.K. Au, F.L. Zhang, Ambient modal identification of a primary-secondary structure by Fast Bayesian FFT method, *Mechanical Systems and Signal Processing* 28 (2012) 280-296.
- [13] S.K. Au., Y.C. Ni, Fast Bayesian modal identification of structures using known single-input forced vibration data, *Structural Control and Health Monitoring* 21(3) (2014) 381-402.
- [14] S.K. Au, F.L. Zhang, On assessing the posterior mode shape uncertainty in ambient modal identification, *Probabilistic Engineering Mechanics* 26(3) (2011) 427-434.
- [15] S.K. Au, C.T. Ng, H.W. Sien, H.Y. Chua, Modal identification of a suspension footbridge using free vibration signatures, *International Journal of Applied Mathematics and Mechanics* 1(4) (2005) 55-73.
- [16] S.K. Au, Assembling mode shapes by least squares, *Mechanical Systems and Signal Processing* 25(1) (2011), 163-179.
- [17] S.K. Au, Connecting Bayesian and frequentist quantification of parameter uncertainty in system identification, *Mechanical Systems and Signal Processing* 29 (2012) 328-342.

Figure Captions

Figure 1 Typical floor plan with measured dofs

Figure 2 Time history, nominal case, synthetic data

Figure 3 Root PSD and SV spectra, nominal case, synthetic data

Figure 4 Identified modal parameters, nominal case, synthetic data

Figure 5 Root PSD spectrum fitting, Method I; solid line represents the measured data, dash line represents the data calculated using identified parameters; the line denotes the selected frequency band

Figure 6 Root PSD spectrum fitting, Method II; solid line represents the measured data, dash line represents the data calculated using identified parameters; the line denotes the selected frequency band

Figure 7 Effect of noise levels, synthetic data (dot: MPV; error bar: ± 2 standard deviation), Method II

Figure 8 Effect of ambient vibration levels, synthetic data (dot: MPV; error bar: ± 2 standard deviation), Method II

Figure 9 Overview of Tanjong Rhu Suspension Bridge

Figure 10 Time history of a typical setup of Mode VA1

Figure 11 Root PSD and SV spectra of a typical setup of Mode VA1

Figure 12 Mode shapes of all the modes under investigation

Figure 13 Root PSD spectrum fitting, Setup 1, VA1; solid line represents the measured data, dash line represents the data calculated using identified parameters; the line denotes the selected frequency band

Figure 14 Error bar of natural frequency and damping ratio, VS1

Figure 15 Error bar of natural frequency and damping ratio, VA1

Figure 16 Error bar of natural frequency and damping ratio, VS2

Figure 17 Error bar of natural frequency and damping ratio, TS1

Figure 18 Overview of CityU Bridge

Figure 19 Setup plan of CityU Bridge

Figure 20 Time history of Setup 1, Mode 1

Figure 21 Root PSD and SV spectra, Mode 1, Setup 1, CityU bridge

Figure 22 Time history of Setup 1, Mode 3

Figure 23 Mode shape, Setup1, Modes 1, 2, 3

Figure 24 Root PSD spectrum fitting, Setup 1, Mode 1; solid line represents the measured data, dash line represents the data calculated using identified parameters; the line denotes the selected frequency band

Figure 25. Error bar of natural frequency and damping ratio with excitation frequencies, Mode 1

Figure 26. Error bar of natural frequency and damping ratio with excitation frequencies, Mode 2

Figure 27. Error bar of natural frequency and damping ratio with excitation frequencies, Mode 3

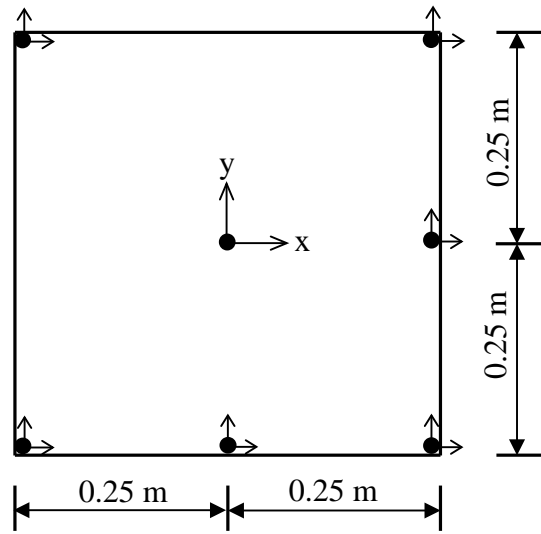


Figure 1 Typical floor plan with measured dofs

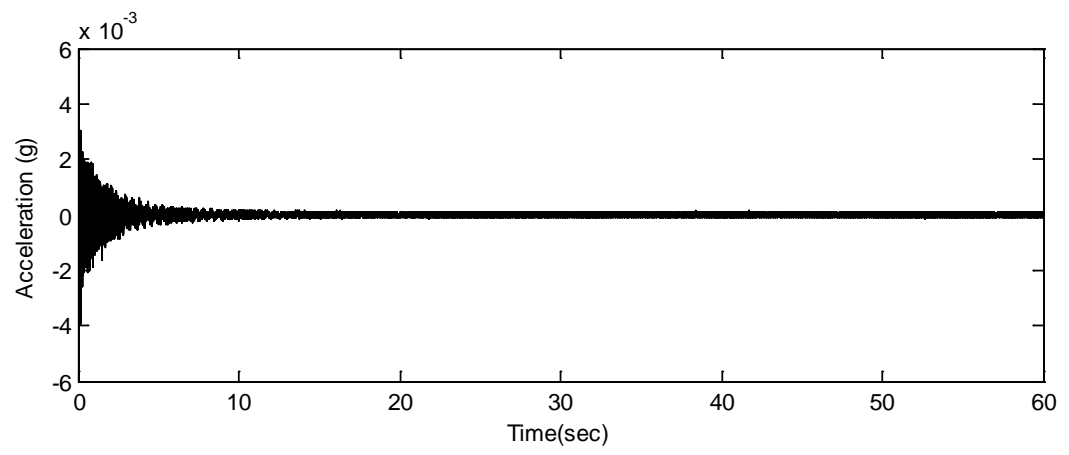


Figure 2 Time history, nominal case, synthetic data

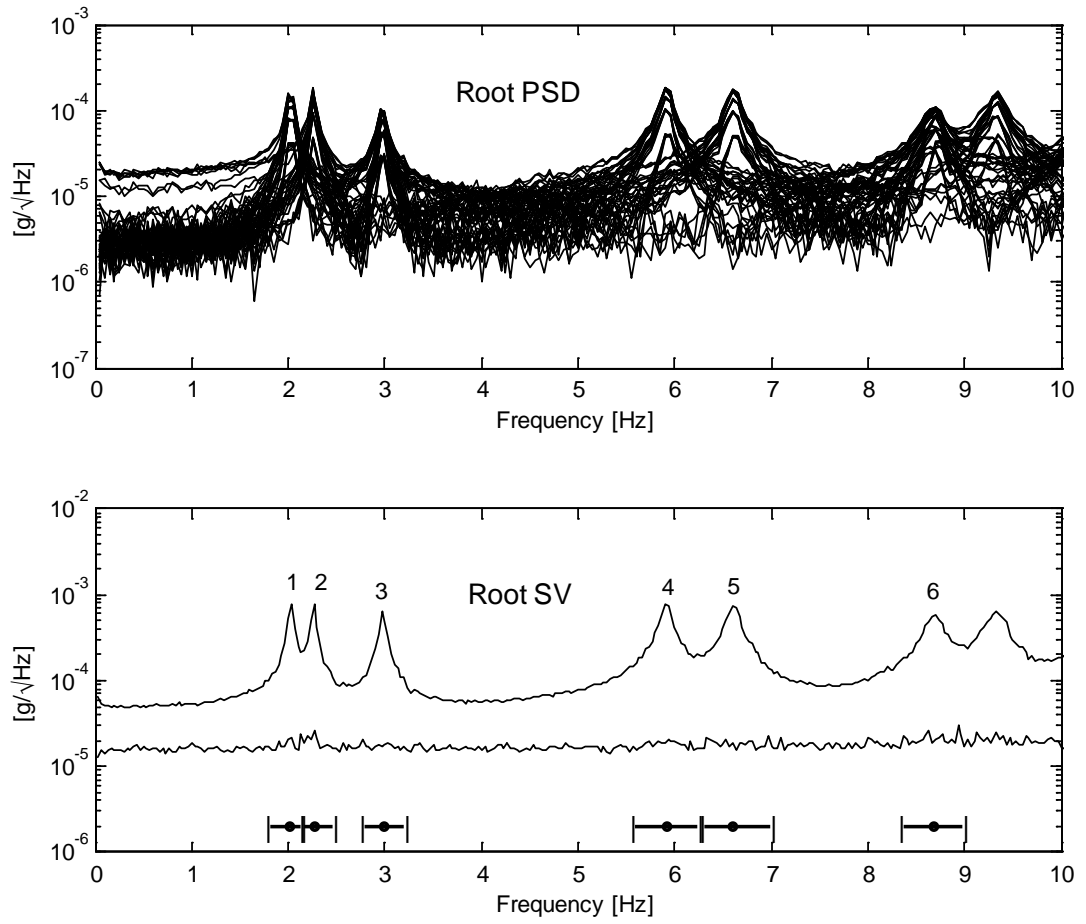
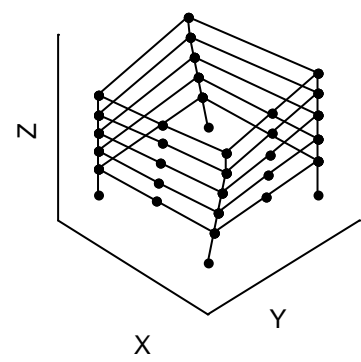
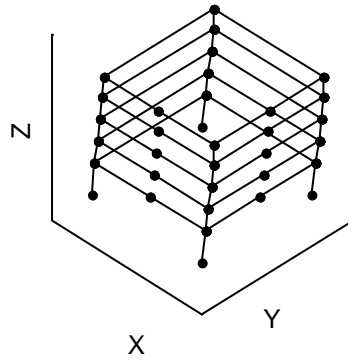
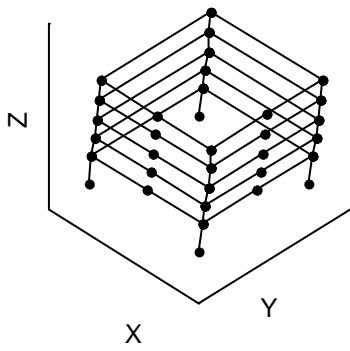


Figure 3 Root PSD and SV spectra, nominal case, synthetic data

Mode 1: 2.026Hz,0.99%

Mode 2: 2.264Hz,0.99%

Mode 3: 2.977Hz,0.99%



Mode 4: 5.915Hz,0.96%

Mode 5: 6.611Hz,1.04%

Mode 6: 8.687Hz,1.00%

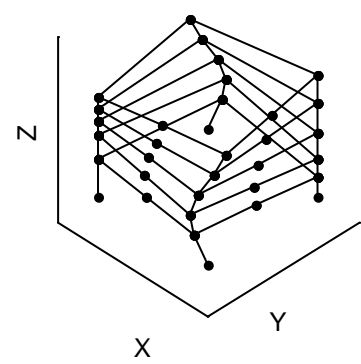
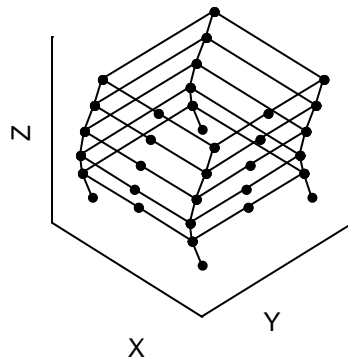
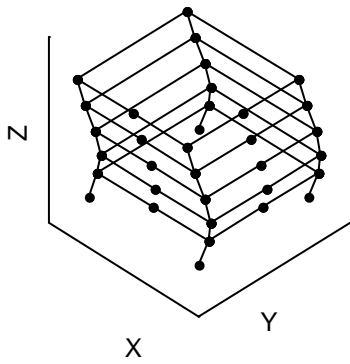


Figure 4 Identified modal parameters, nominal case, synthetic data

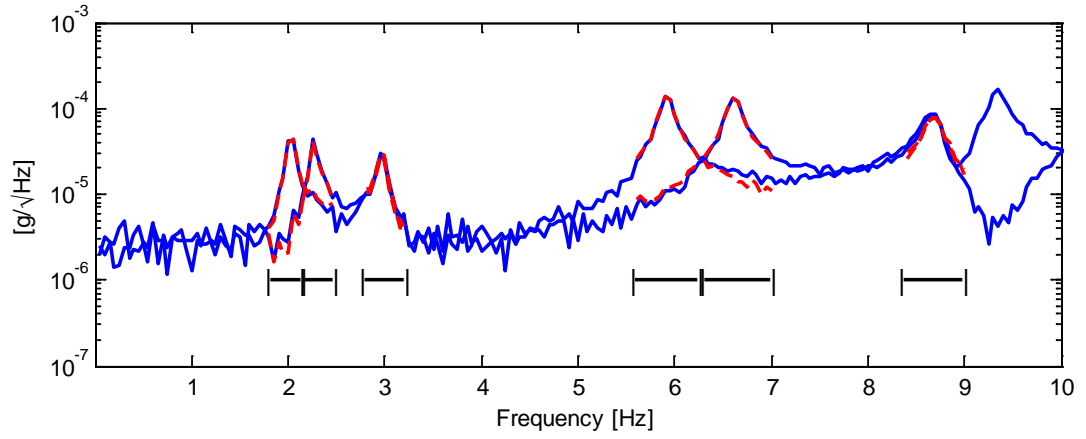


Figure 5 Root PSD spectrum fitting, Method I; solid line represents the measured data, dash line represents the data calculated using identified parameters; the line denotes the selected frequency band

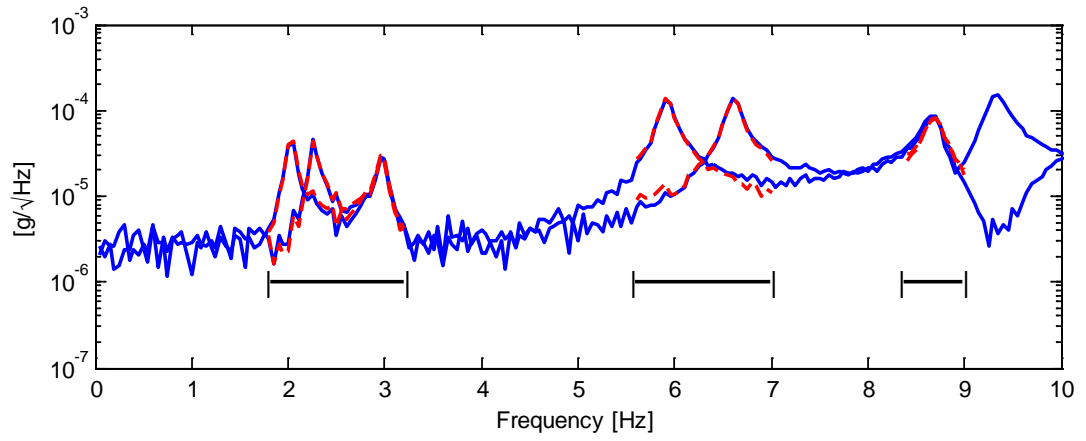


Figure 6 Root PSD spectrum fitting, Method II; solid line represents the measured data, dash line represents the data calculated using identified parameters; the line denotes the selected frequency band

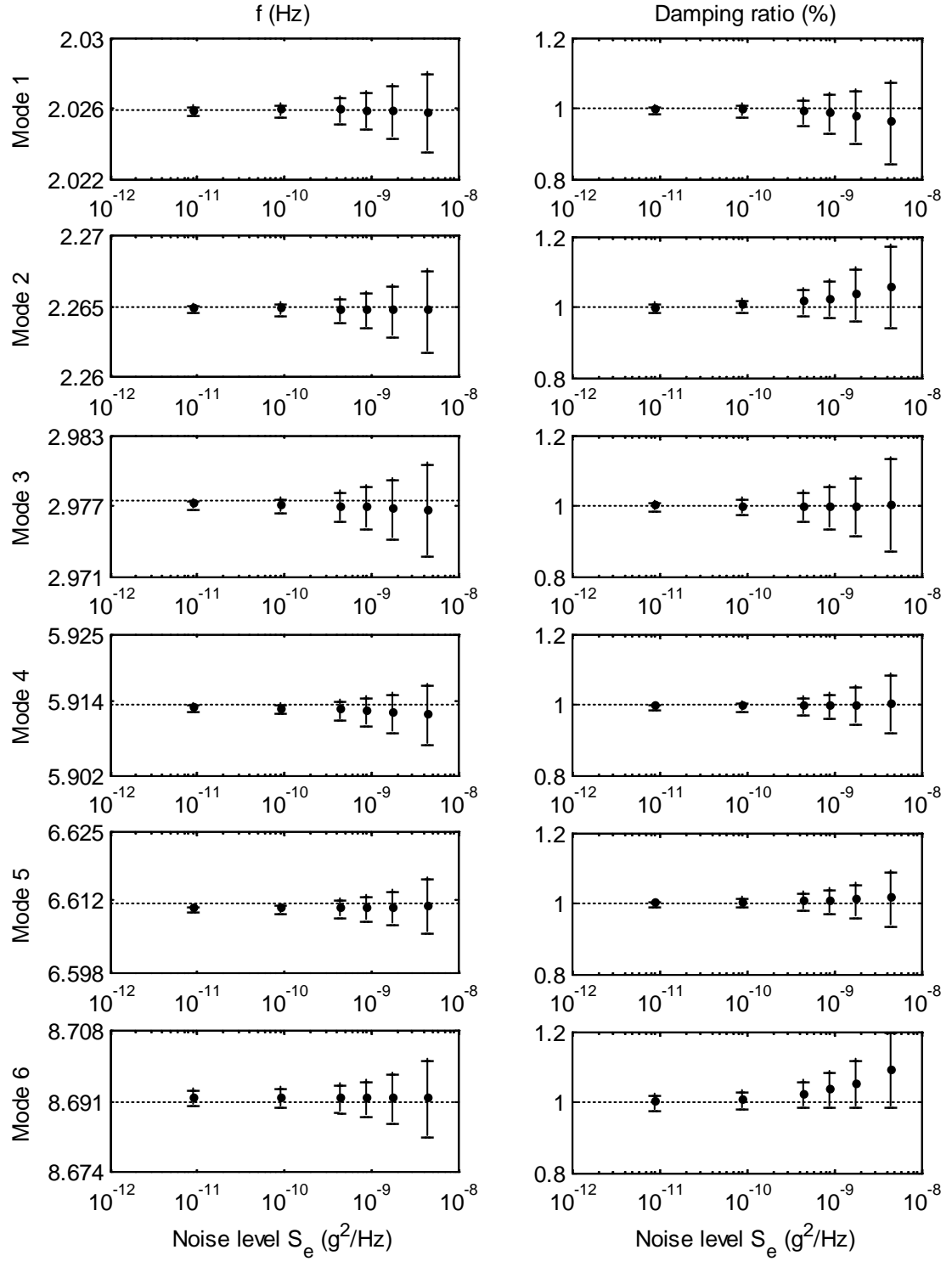


Figure 7 Effect of noise levels, synthetic data (dot: MPV; error bar: ± 2 standard deviation), Method II

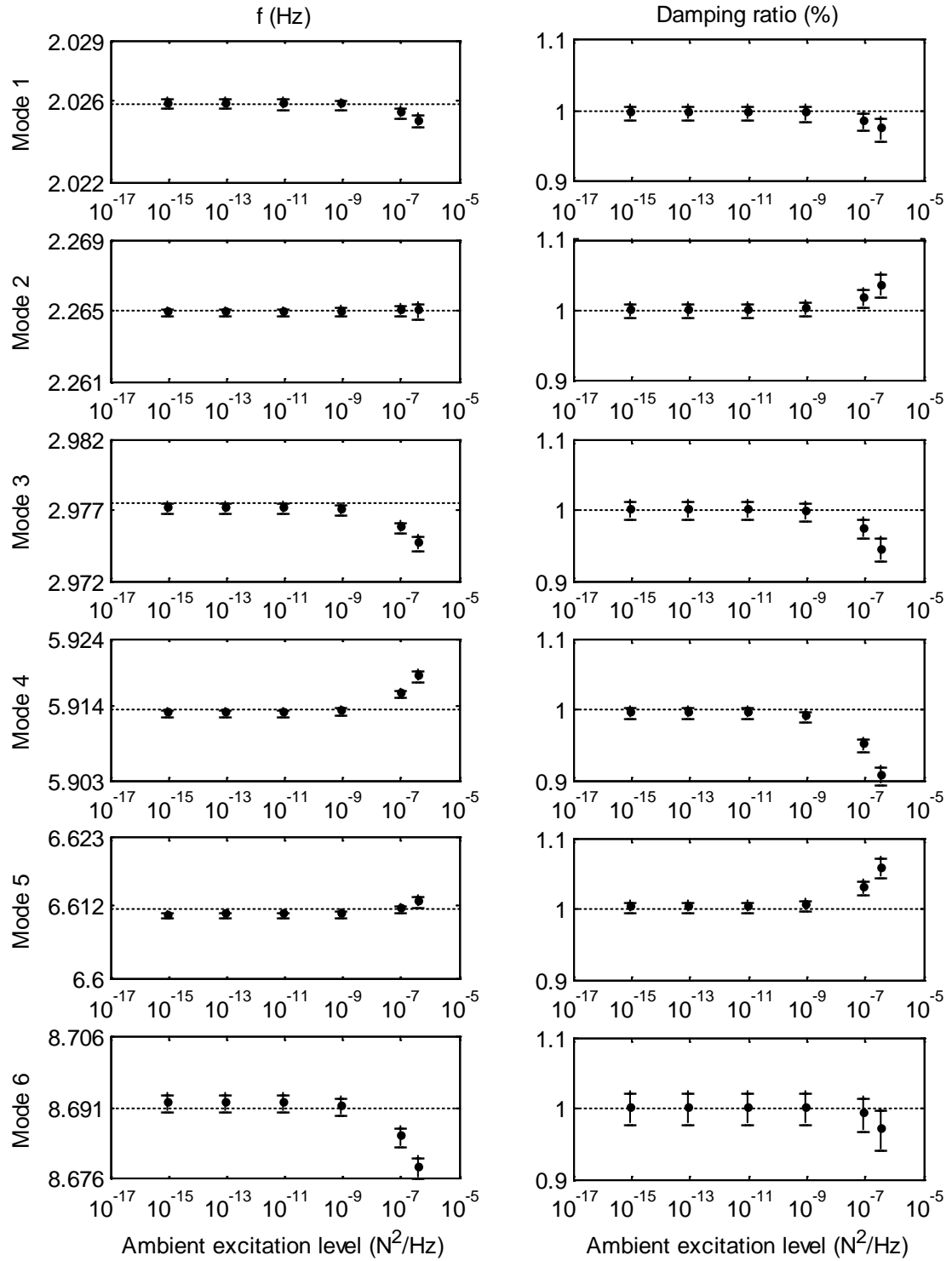


Figure 8 Effect of ambient vibration levels, synthetic data (dot: MPV; error bar: ± 2 standard deviation), Method II



Figure 9 Overview of Tanjong Rhu Suspension Bridge

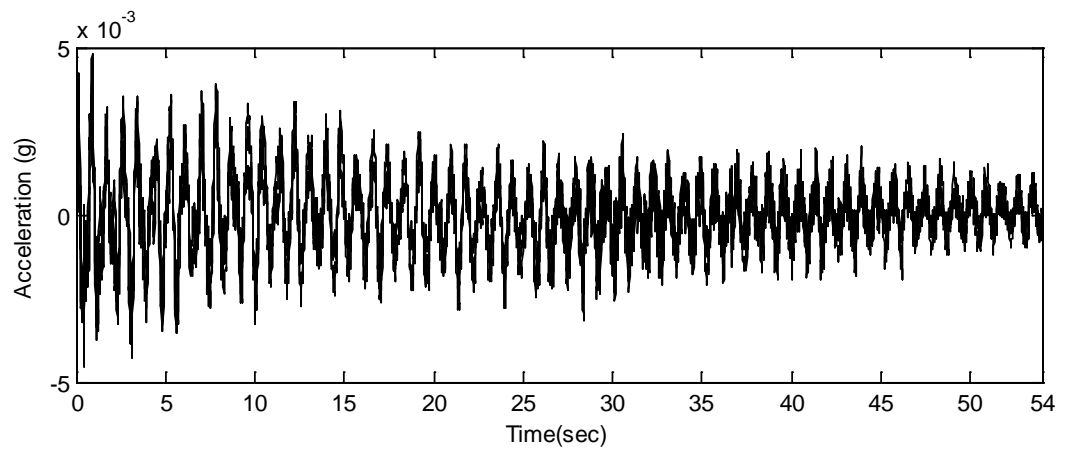


Figure 10 Time history of a typical setup of Mode VA1

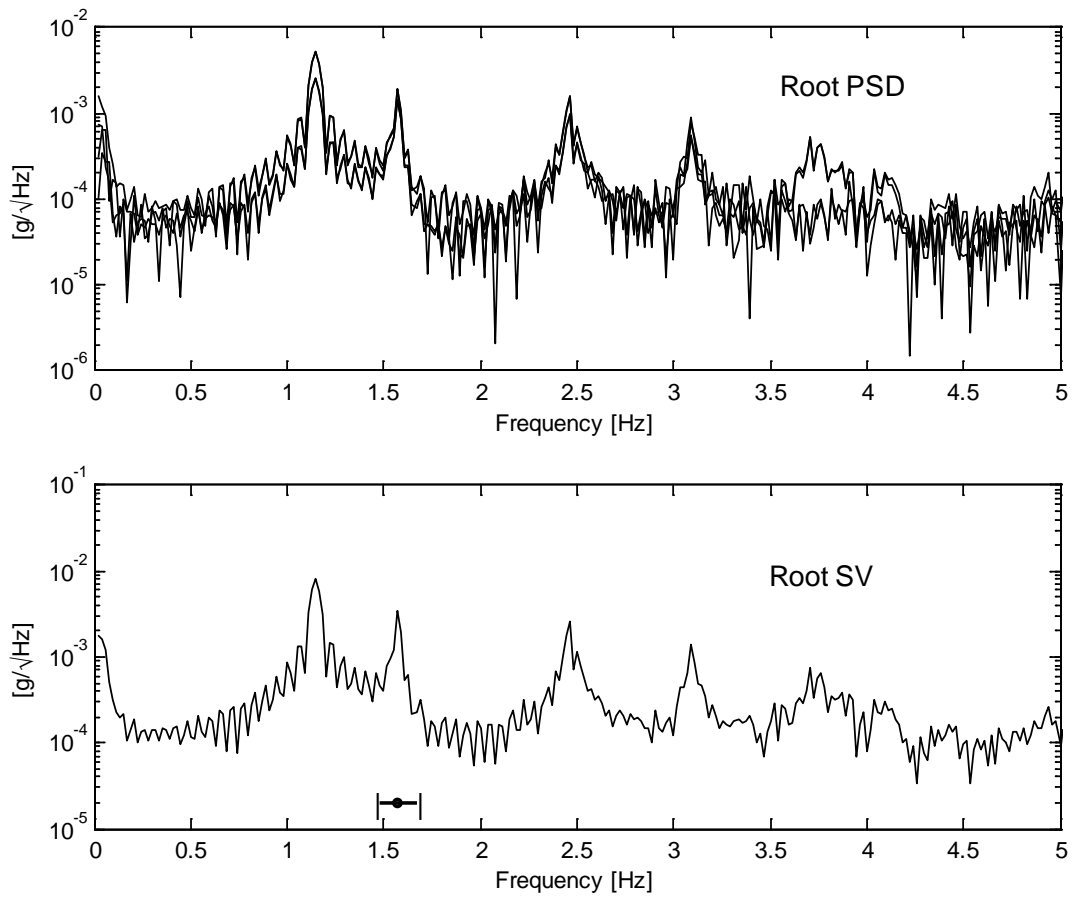
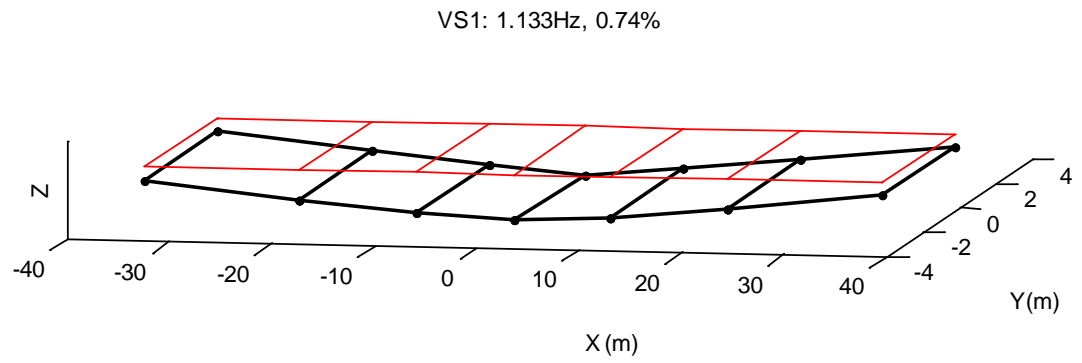
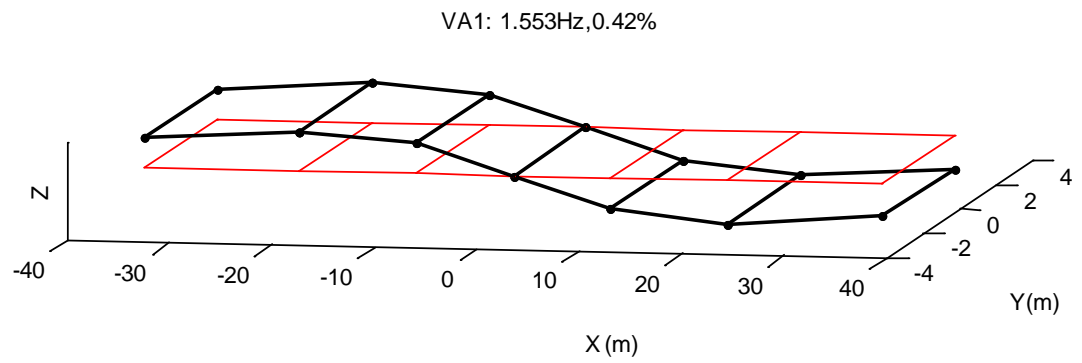


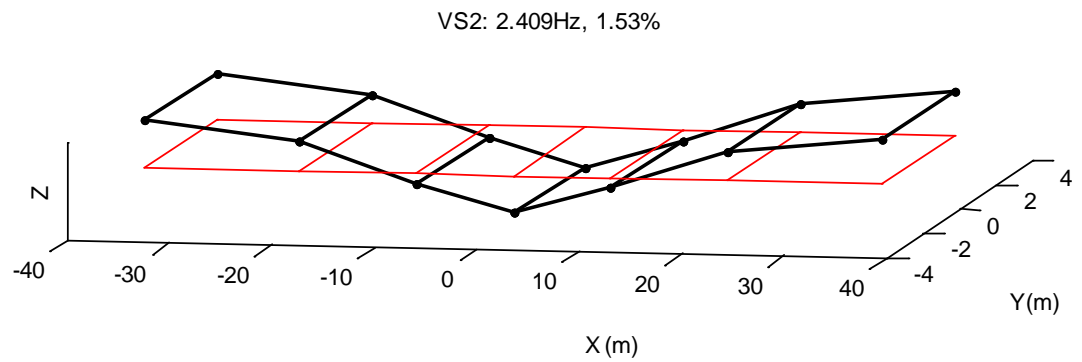
Figure 11 Root PSD and SV spectra of a typical setup of Mode VA1



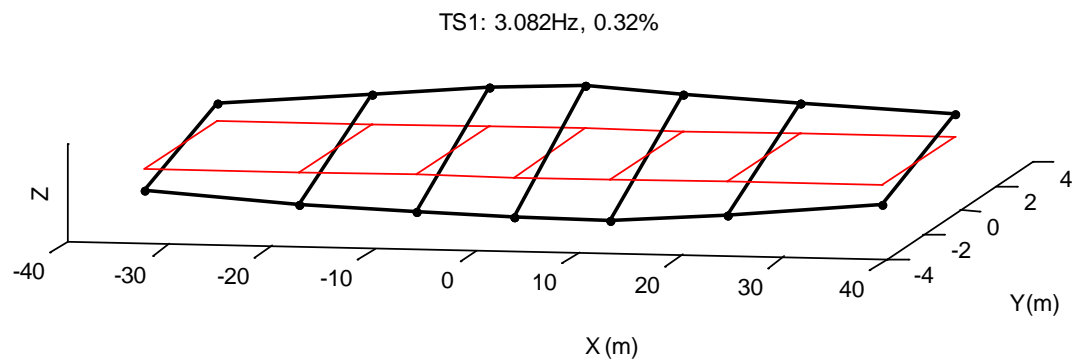
Mode 1



Mode 2



Mode 3



Mode 4

Figure 12 Mode shapes of all the modes under investigation

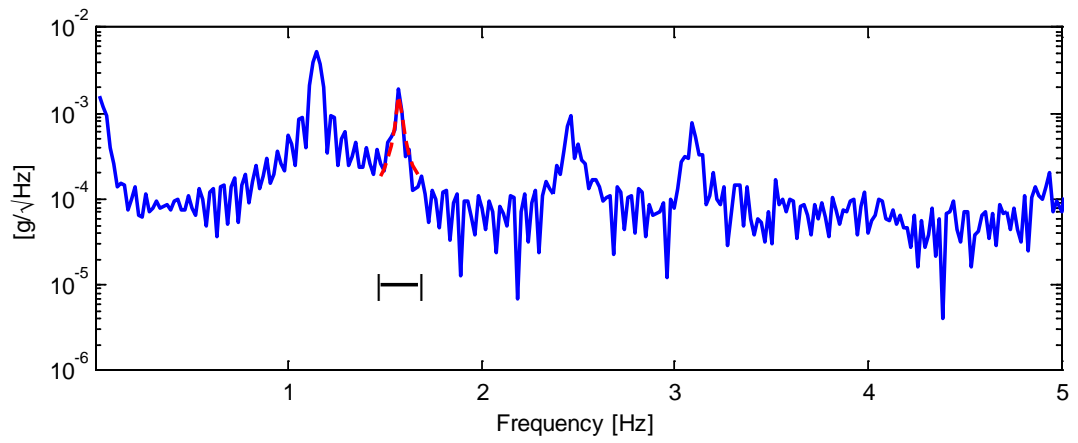


Figure 13 Root PSD spectrum fitting, Setup 1, VA1; solid line represents the measured data, dash line represents the data calculated using identified parameters; the line denotes the selected frequency band

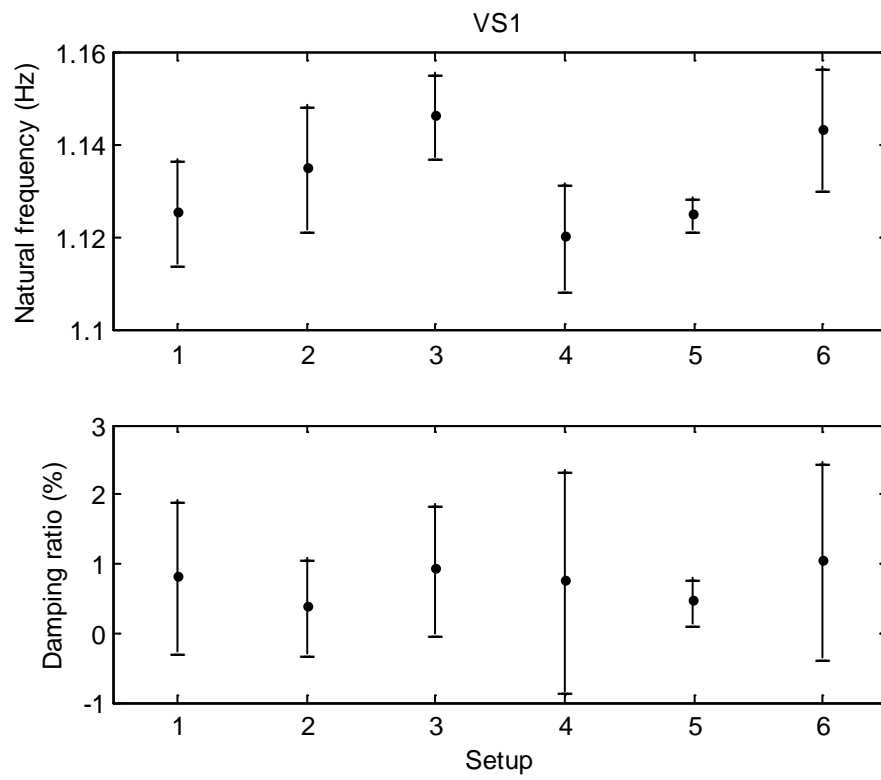


Figure 14 Error bar of natural frequency and damping ratio, VS1

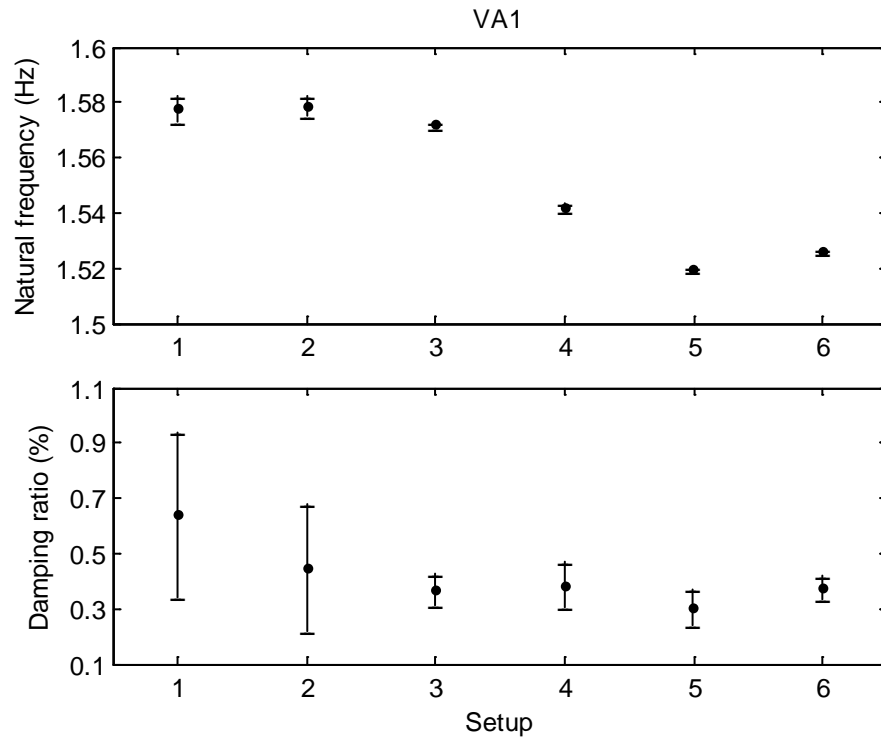


Figure 15 Error bar of natural frequency and damping ratio, VA1

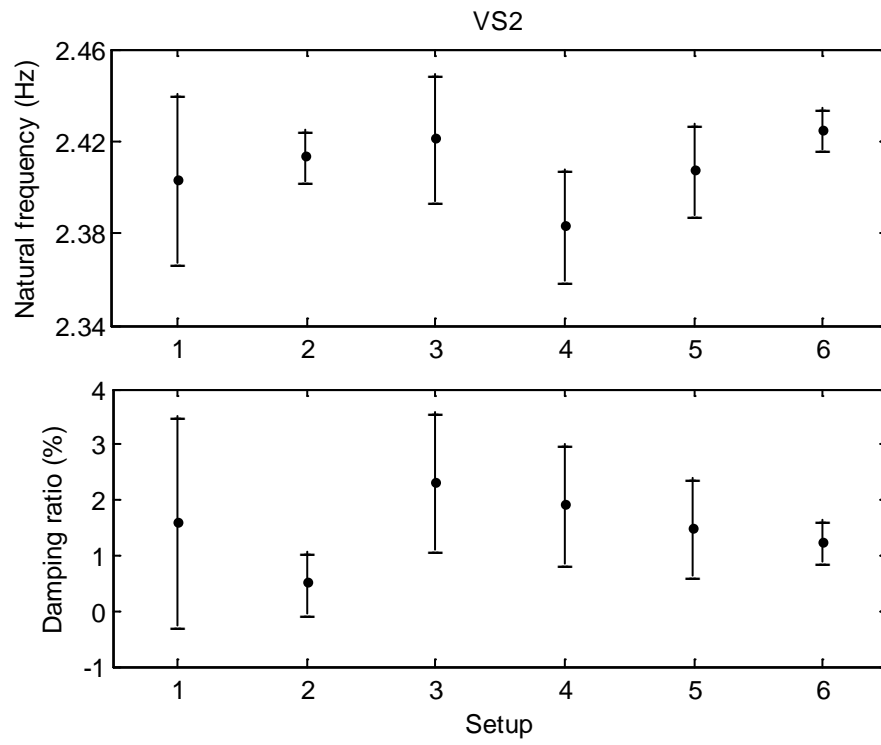


Figure 16 Error bar of natural frequency and damping ratio, VS2

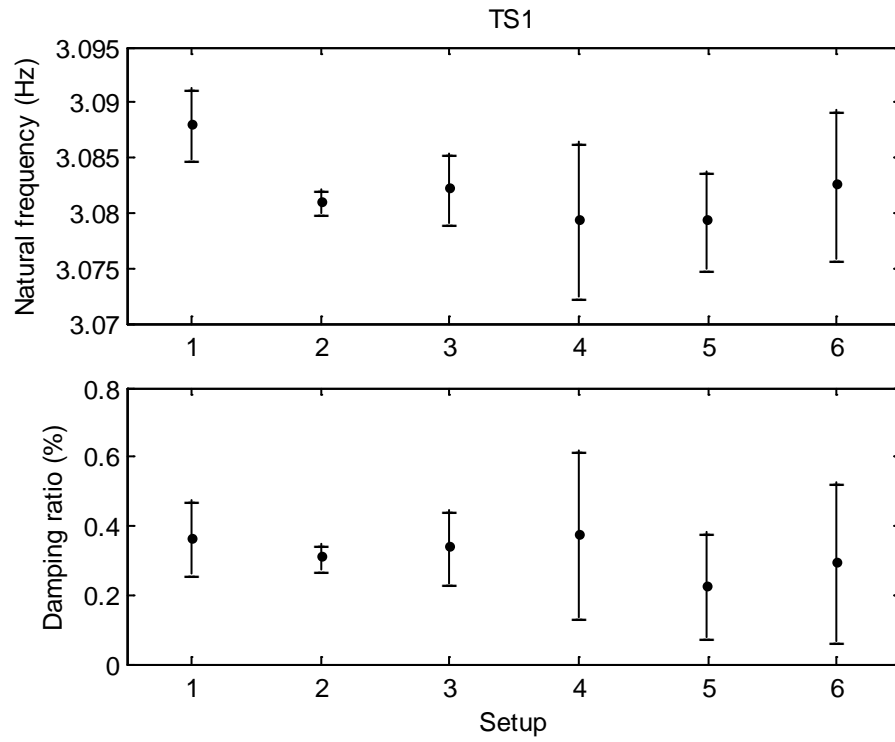


Figure 17 Error bar of natural frequency and damping ratio, TS1



Figure 18 Overview of CityU Bridge

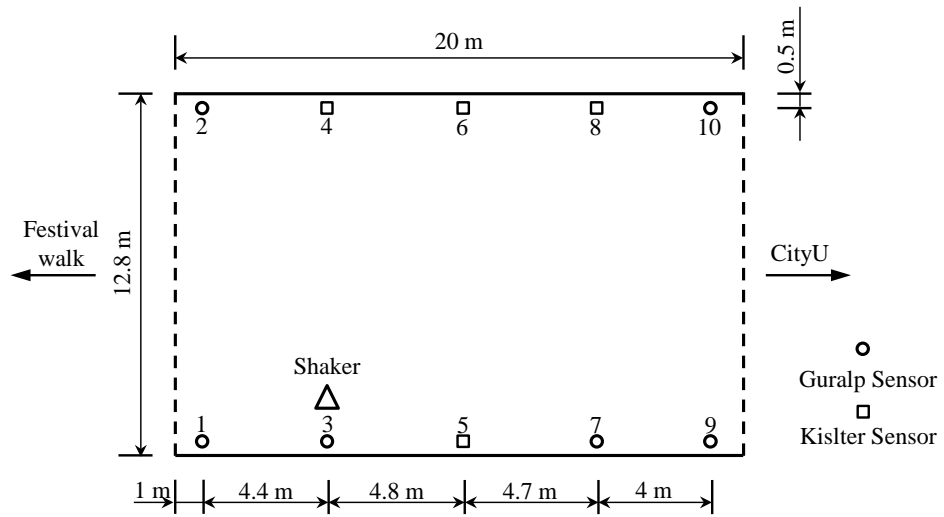


Figure 19 Setup plan of CityU Bridge

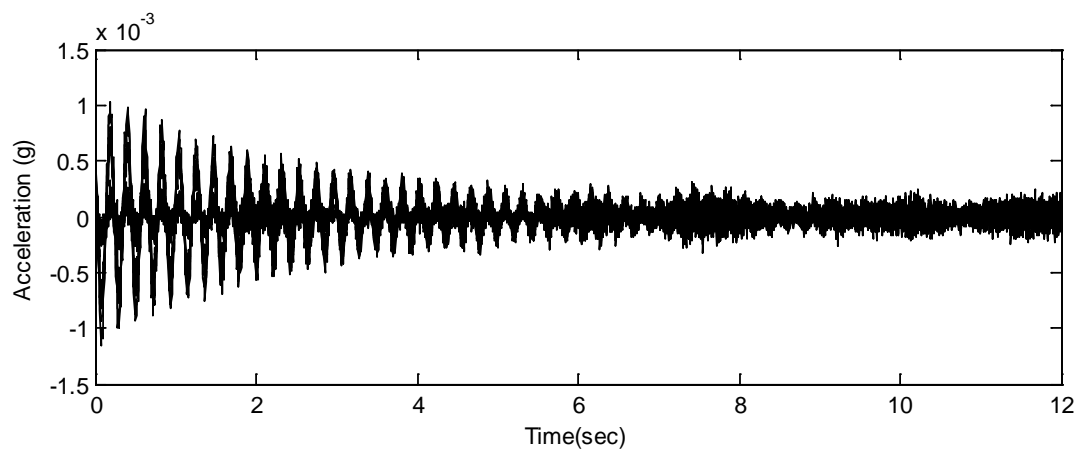


Figure 20 Time history of Setup 1, Mode 1

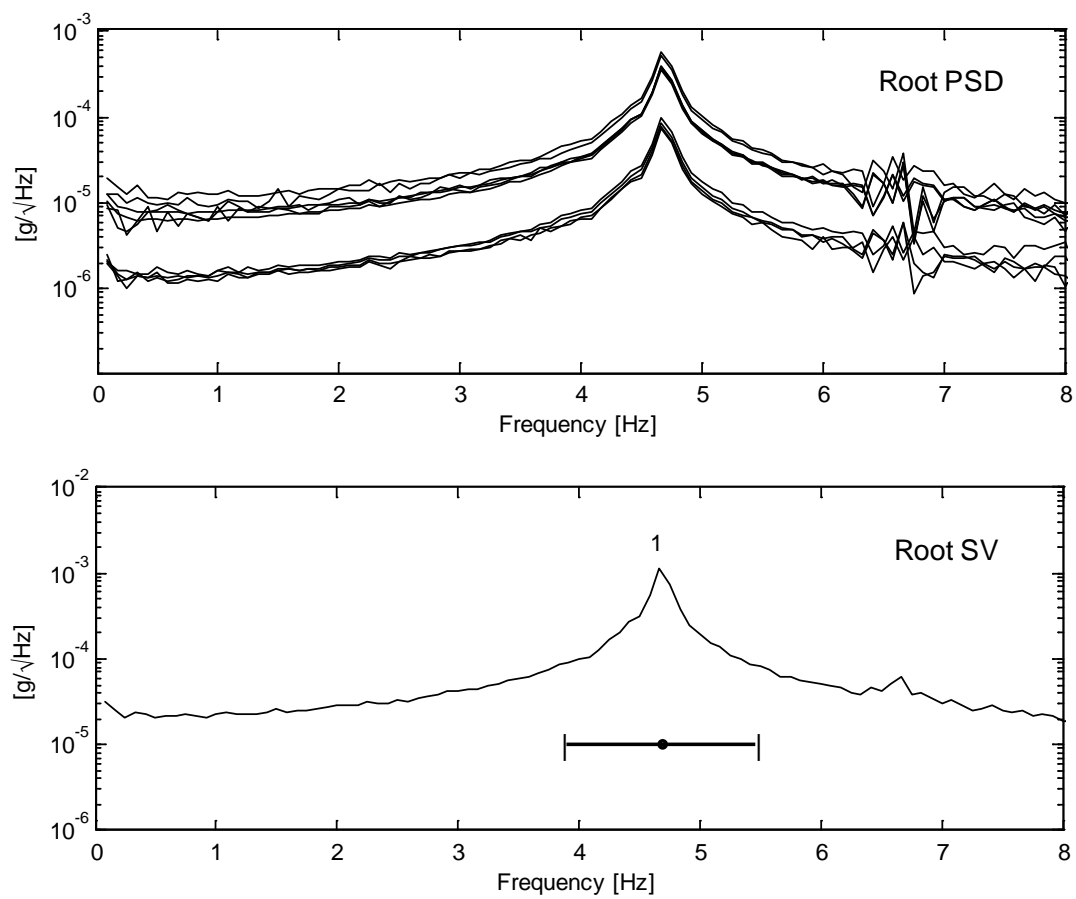


Figure 21 Root PSD and SV spectra, Mode 1, Setup 1, CityU bridge

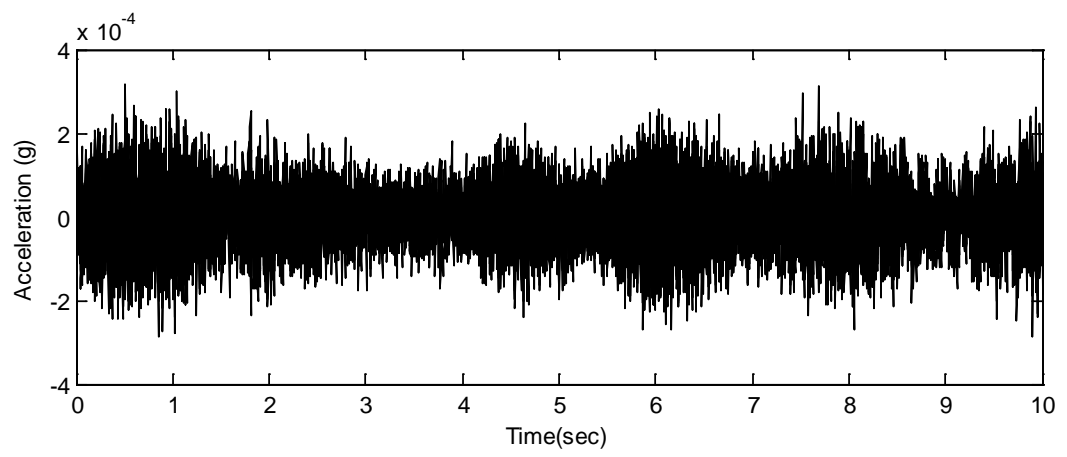


Figure 22 Time history of Setup 1, Mode 3

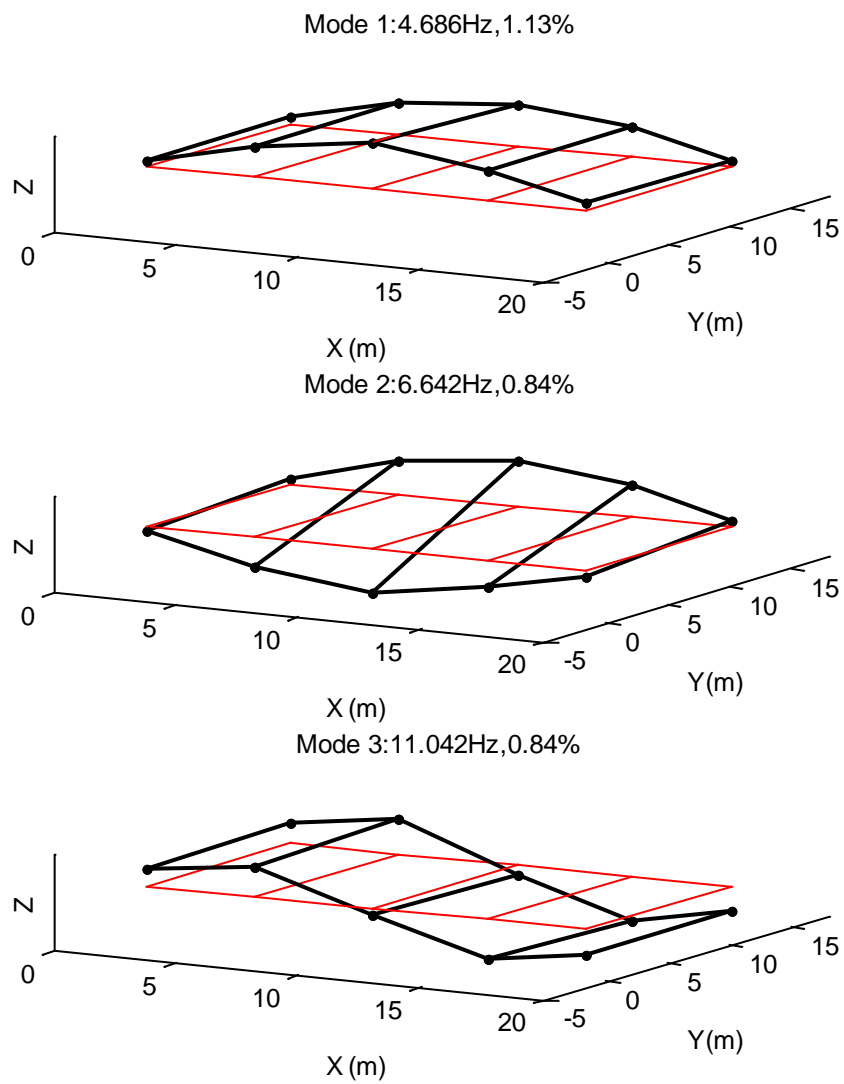


Figure 23 Mode shape, Setup1, Modes 1, 2, 3

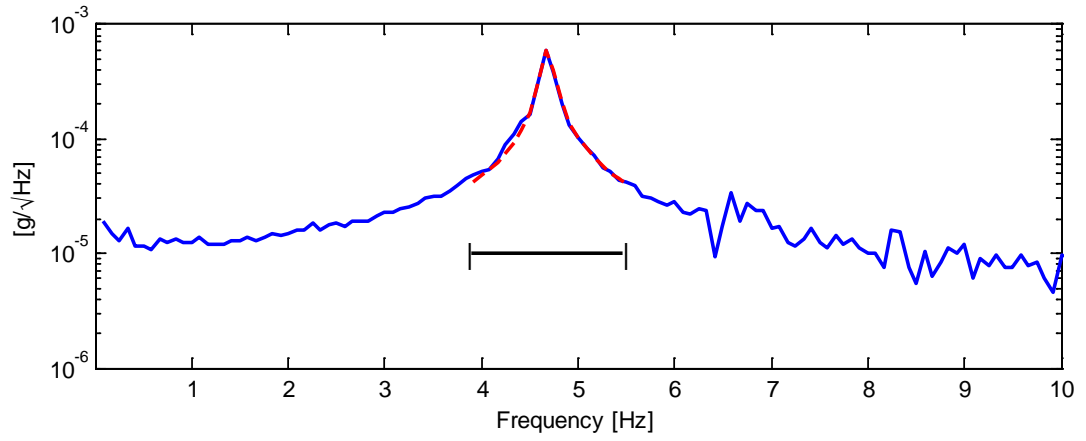


Figure 24 Root PSD spectrum fitting, Setup 1, Mode 1; solid line represents the measured data, dash line represents the data calculated using identified parameters; the line denotes the selected frequency band

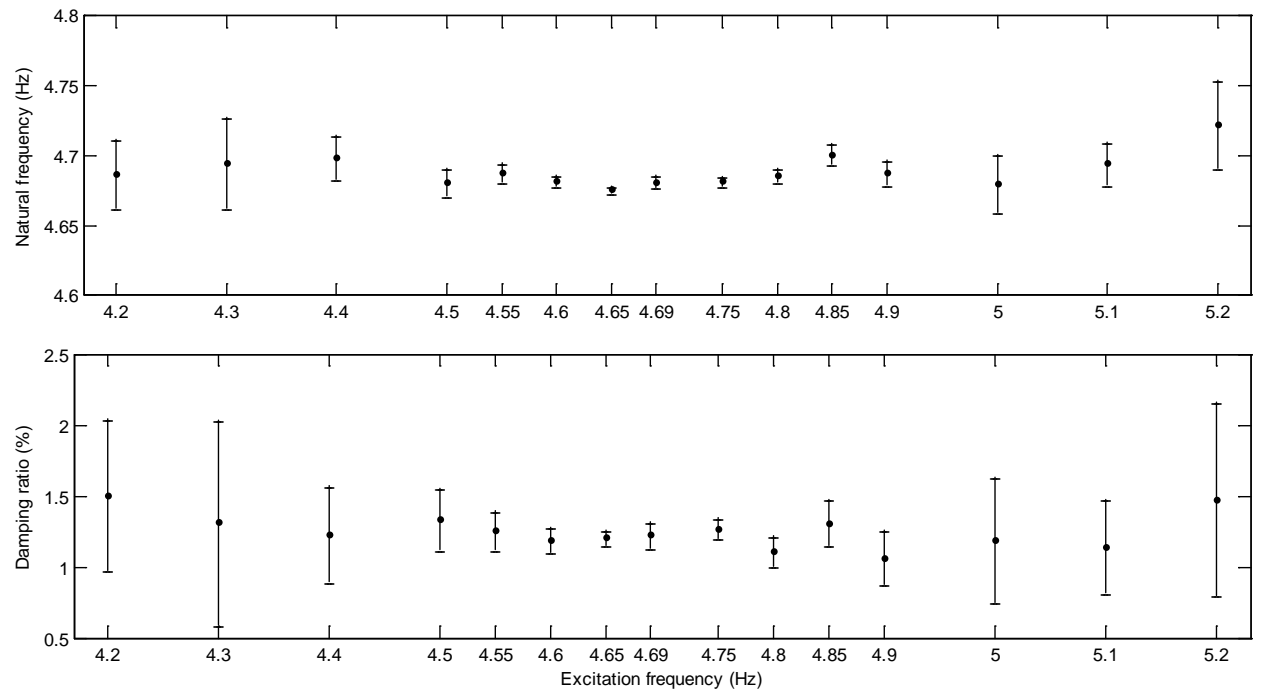


Figure 25. Error bar of natural frequency and damping ratio with excitation frequencies, Mode 1

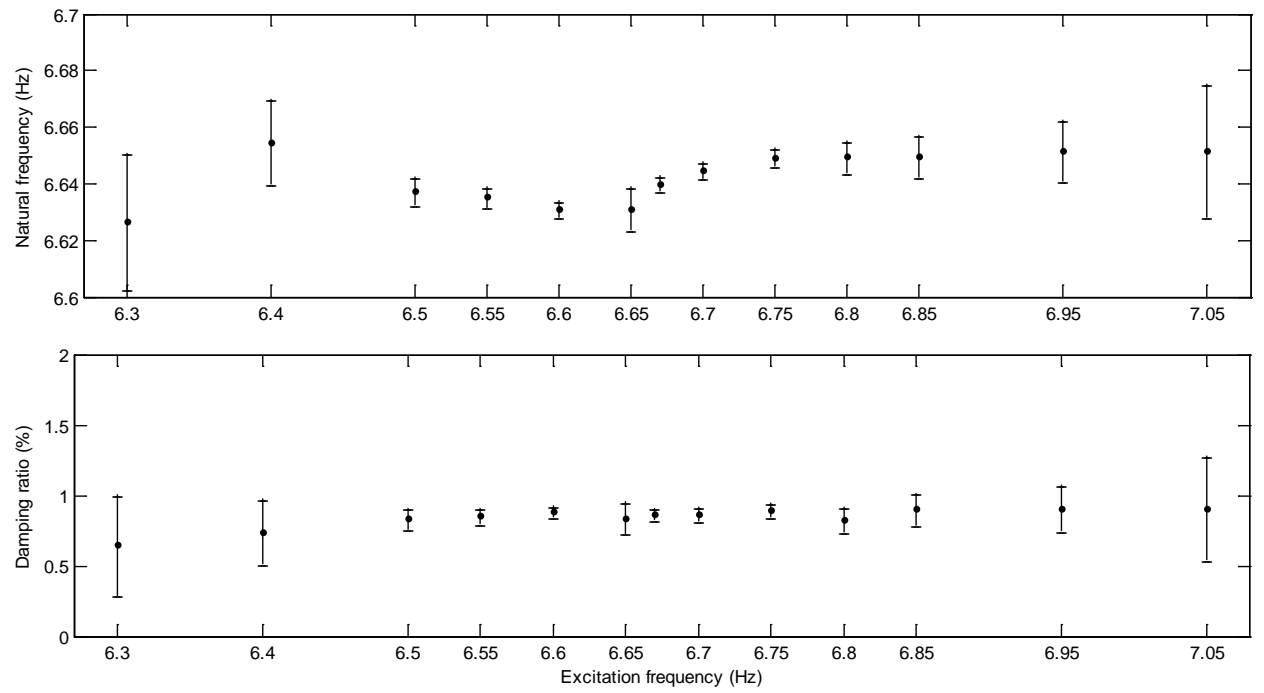


Figure 26. Error bar of natural frequency and damping ratio with excitation frequencies, Mode 2

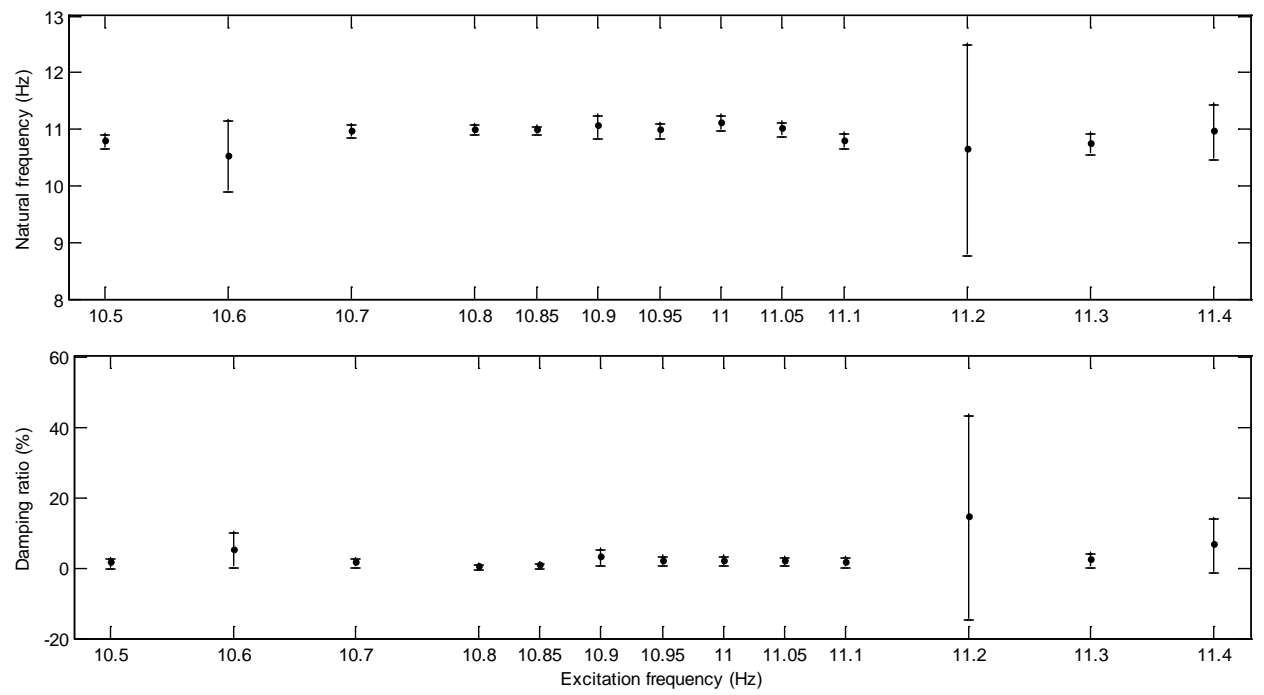


Figure 27. Error bar of natural frequency and damping ratio with excitation frequencies, Mode 3

Table 1 Initial conditions, Displacement: m; Velocity: 10^{-3} m/s

Mode	1	2	3	4	5	6	7	8	9	10	11	12	13	14	15
Dis.	0	0	0	0	0	0	0	0	0	0	0	0	0	0	0
Vel.	0.36	0.36	0.86	0.33	0.33	0.79	0.27	0.27	-0.20	-0.20	-0.10	0.66	-0.10	-0.47	-0.24

Table 2 Exact values of modal parameters for synthetic data

Mode	f (Hz)	ζ (%)	S (10^{-12} g^2/Hz)	S_e (10^{-12} g^2/Hz)	u (10^{-3} g)	v (10^{-3} g/s)
1	2.026	1.00	2.24	9.00	-0.023	-14.5
2	2.265	1.00	2.24	9.00	-0.026	-18.1
3	2.977	1.00	2.10	9.00	-0.026	-24.2
4	5.914	1.00	2.24	9.00	-0.061	-113.4
5	6.612	1.00	2.24	9.00	-0.068	-141.8
6	8.691	1.00	2.10	9.00	-0.070	-189.7

Table 3 Identified parameters for synthetic data (Method I)

Mode	γ	f		ζ		S		S_e		u		v		Φ	
		MPV (Hz)	c.o.v. (%)	MPV (%)	c.o.v. (%)	MPV (10^{-12} g^2/Hz)	c.o.v. (%)	MPV (10^{-12} g^2/Hz)	c.o.v. (%)	MPV (10^{-3} g)	c.o.v. (%)	MPV (10^{-3} g/s)	c.o.v. (%)	MAC	1-EMAC 10^{-4}
1	3657	2.026	0.034	0.99	3.46	1.49	32	155.74	2.9	-0.008	255	-14.6	1.8	0.9999	9.2
2	6361	2.264	0.044	0.99	4.46	2.66	28	114.09	3.1	-0.072	38	-17.3	2.3	0.9999	6.8
3	15069	2.977	0.036	0.99	3.61	1.56	25	54.30	2.7	-0.039	59	-24.1	1.8	0.9999	3.7
4	4390	5.915	0.023	0.96	2.43	1.56	21	168.67	2.1	-0.053	76	-112.7	1.3	0.9999	4.3
5	6233	6.611	0.024	1.04	2.30	1.72	19	116.68	2.0	-0.053	81	-142.7	1.3	0.9999	2.9
6	2707	8.687	0.032	1.00	3.22	1.92	21	272.47	2.1	-0.084	84	-185.1	2.1	0.9999	8.8

Table 4 Identified parameters for synthetic case (Method II)

Mode	γ	f		ζ		S_e		u		v		Φ	
		MPV (Hz)	c.o.v. (%)	MPV (%)	c.o.v. (%)	MPV (10^{-12} g^2/Hz)	c.o.v. (%)	MPV (10^{-3}g)	c.o.v. (%)	MPV (10^{-3}g/s)	c.o.v. (%)	MAC	1-EMAC (10^{-4})
1	12633	2.026	0.006	0.99	0.6	50	1.4	-0.008	69.7	-14.8	0.4	0.9997	2.9
2	12633	2.265	0.006	1.02	0.6	50	1.4	-0.055	10.5	-18.0	0.4	0.9999	2.8
3	12633	2.976	0.007	0.98	0.7	50	1.4	-0.051	12.7	-24.5	0.5	0.9991	3.3
4	9518	5.916	0.005	0.95	0.5	67	1.4	-0.003	351.6	-112.1	0.3	0.9997	1.6
5	9518	6.612	0.005	1.03	0.5	67	1.4	-0.061	19.6	-142.0	0.3	0.9998	1.6
6	2119	8.685	0.012	0.99	1.2	299	2.1	-0.150	21.3	-187.2	0.9	0.9999	9.8

Table 5 Identified parameters for Tanjong Bridge (Method I)

Mode	γ	f		ζ		S		S_e		Φ
										1-EMAC (10^{-4})
		MPV (Hz)	c.o.v. (%)	MPV (%)	c.o.v. (%)	MPV (10^{-9} g^2/Hz)	c.o.v. (%)	MPV (10^{-9} g^2/Hz)	c.o.v. (%)	
VS1	9411	1.126	0.50	0.83	66	28.57	34	10.15	18	0.4
VA1	1292	1.578	0.15	0.64	24	0.28	32	1.29	17	0.5
VS2	22059	2.404	0.76	1.61	58	10.42	46	4.51	17	1.1
TS1	3148	3.088	0.05	0.37	14	0.31	40	34.35	18	1.3

Table 6 Identified parameters for Tanjong Bridge (Setup1) (Method II)

Mode	γ	f		ζ		S_e		Φ
		MPV (Hz)	c.o.v. (%)	MPV (%)	c.o.v. (%)	MPV (10^{-9} g^2/Hz)	c.o.v. (%)	1-EMAC (10^{-4})
VS1	633	1.132	0.05	0.25	18.7	247.19	15.8	11.5
VA1	711	1.579	0.02	0.45	4.7	15.71	12.2	6.3
VS2	743	2.415	0.09	0.48	14.4	210.74	15.1	75.4
TS1	541	3.087	0.02	0.34	6.3	273.60	10.2	10.0

Table 7 Identified parameters for CityU Bridge (Method I)

Mode	γ	f		ζ		S		S_e		Φ
		MPV (Hz)	c.o.v. (%)	MPV (%)	c.o.v. (%)	MPV (10^{-12} g ² /Hz)	c.o.v. (%)	MPV (10^{-12} g ² /Hz)	c.o.v. (%)	1-EMAC (10^{-4})
1	17817	4.682	0.05	1.23	3.8	4.01	25.4	23.24	7.4	0.2
2	20737	6.640	0.02	0.87	2.3	2.04	36.0	168.39	8.5	0.4
3	52	10.993	0.62	2.34	31.4	5.13	40.4	42.98	8.6	36.2

Table 8 Identified parameters for CityU Bridge (Method II)

Mode	γ	f		ζ		S_e		Φ
		MPV (Hz)	c.o.v. (%)	MPV (%)	c.o.v. (%)	MPV (10^{-12} g^2/Hz)	c.o.v. (%)	1-EMAC (10^{-4})
1	19875	4.686	0.008	1.13	0.7	63.17	7.1	0.5
2	13423	6.642	0.006	0.84	0.8	258.46	8.2	0.6
3	64	11.042	0.103	0.84	8.7	94.85	8.2	108.4